Effectiveness of a novel polyaniline@Fe-ZSM-5 hybrid composite for Orange G dye removal from aqueous media: Experimental study and advanced statistical physics insights

Abdelaziz Imgharn, Lahoucine Anchoum, Abdelghani Hsini, Yassine Naciri, Mohamed Laabd, Mohamed Mobarak, Nouh Aarab, Asmae Bouziani, Sabine Szunerits, Rabah Boukherroub, et al.

Journal Pre-proof

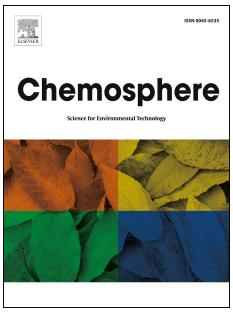

Effectiveness of a novel polyaniline@Fe-ZSM-5 hybrid composite for Orange G dye removal from aqueous media: Experimental study and advanced statistical physics insights

Abdelaziz Imgharn, Lahoucine Anchoum, Abdelghani Hsini, Yassine Naciri, Mohamed Laabd, Mohamed Mobarak, Nouh Aarab, Asmae Bouziani, Sabine Szunerits, Rabah Boukherroub, Rajae Lakhmiri, Abdallah Albourine

PII: S0045-6535(22)00279-X

DOI: https://doi.org/10.1016/j.chemosphere.2022.133786

Reference: CHEM 133786

To appear in: *ECSN*

Received Date: 25 September 2021

Revised Date: 5 January 2022

Accepted Date: 27 January 2022

Please cite this article as: Imgharn, A., Anchoum, L., Hsini, A., Naciri, Y., Laabd, M., Mobarak, M., Aarab, N., Bouziani, A., Szunerits, S., Boukherroub, R., Lakhmiri, R., Albourine, A., Effectiveness of a novel polyaniline@Fe-ZSM-5 hybrid composite for Orange G dye removal from aqueous media: Experimental study and advanced statistical physics insights, *Chemosphere* (2022), doi: https://doi.org/10.1016/j.chemosphere.2022.133786.

Author Contributions Statement

Abdelaziz Imgharn: Formal analysis, Data curation, Writing-original draft. **Lahoucine Anchoum:** Investigation. **Abdelghani Hsini:** Methology, Formal analysis, Data curation, Writing-review & editing. **Yassine Naciri:** Methodology, Investigation, Writing-review & editing. **Mohamed Laabd:** Validation, Writing-review & editing. **Mohamed Mobarak:** Formal analysis, Data curation. **Nouh Aarab:** Investigation. **Asmae Bouziani:** Writing-review & editing. **Sabine Szunerits:** Investigation, Methodology. **Rabah Boukherroub:** Conceptualization, Validation, Writing-review & editing. **Rajae Lakhmiri:** revision, editing. **Abdallah Albourine:** Conceptualization, Validation, revision, editing, Supervision, Project administration.

Graphical abstract

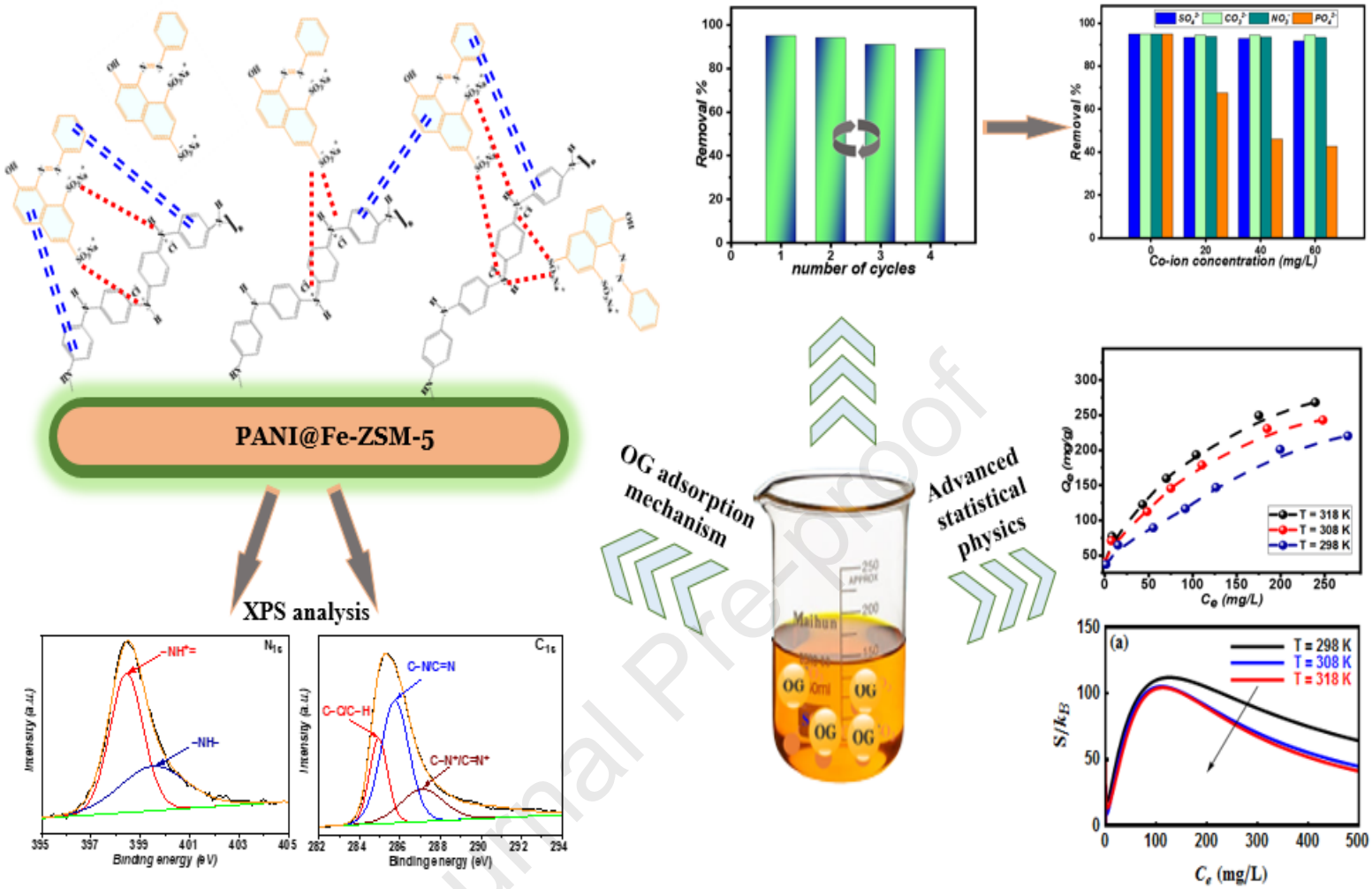

Effectiveness of a novel polyaniline@Fe-ZSM-5 hybrid composite for Orange G dye removal from aqueous media: Experimental study and advanced statistical physics insights

Abdelaziz Imgharn[a], *, Lahoucine Anchoum[a], Abdelghani Hsini[a], Yassine Naciri[a] , Mohamed Laabd[a], Mohamed Mobarak [b], Nouh Aarab[a], Asmae Bouziani[c], Sabine Szunerits[d], Rabah Boukherroub[d], Rajae Lakhmiri[e], Abdallah Albourine[a,*]

[a] *Laboratory of Materials and Environment, Faculty of Sciences, Ibn Zohr University, Agadir, Morocco.*

[b] *Physics Department, Faculty of Science, Beni-Suef University, Beni-Suef 62511, Egypt.*

[c] *Chemical Engineering Department, Middle East Technical University, Ankara, Turkey.*

[d] *Univ. Lille, CNRS, Centrale Lille, Univ. Polytechnique Hauts-de-France, UMR 8520 - IEMN, Lille F-59000, France.*

[e] *Laboratory of Chemical Engineering and Valorization Resources, Faculty of Sciences and Techniques, Abdelmalek Essaadi University, Tangier, Morocco.*

[*] Corresponding authors:

E-mail address: abdelaziz.imgharn@edu.uiz.ac.ma (A. Imgharn)

E-mail address: albourine@yahoo.fr (A. Albourine)

Abstract

A polyaniline@Fe-ZSM-5 composite was synthesized *via* an *in situ* interfacial polymerization procedure. The morphology, crystallinity, and structural features of the as-developed PANI@Fe-ZSM-5 composite were assessed using scanning electron microscopy – energy dispersive spectroscopy (SEM-EDS), X-ray diffraction (XRD), Fourier-transform infrared (FTIR) spectroscopy, and X-ray photoelectron spectroscopy (XPS). The composite was efficiently employed for the first time as an adsorbent ~~to adsorb~~ Orange G (OG) dyestuff from water. The OG dye adsorption performance was investigated as a function of several operating conditions. The kinetic study demonstrated that a pseudo-second-order model was appropriate to anticipate the OG adsorption process. The maximum adsorption capacity was found to be 217 mg/g. The adsorption equilibrium data at different temperatures were calculated *via* advanced statistical physics formalism. The entropy function indicated that the disorder of OG molecules improved at low concentrations and lessened at high concentrations. The free enthalpy and internal energy functions suggested that the OG adsorption was a spontaneous process and physisorption in nature. Regeneration investigation showed that the PANI@Fe-ZSM-5 could be effectively reused up to five cycles. The main results of this work provided a deep insight on the experimental study supported by advanced statistical physics prediction for the adsorption of Orange G dye onto the novel polyaniline@Fe-ZSM-5 hybrid composite. Additionally, the experimental and advanced statistical physics findings stated in this study may arouse research interest in the field of wastewater treatment.

Keywords: Polyaniline; Fe-ZSM-5; Composite; Dye removal; Advanced statistical physics; Regeneration.

1. Introduction

Many industries use synthetic dyes to color their final product, including food, drugs, cosmetics, paper, leather, plastics, and textile (Abbasi, 2017). Dyes often exhibit persistence to biodegradation and significant toxic, carcinogenic, and mutagenic effects on aquatic organisms and humans, which has become a severe environmental problem in the world (Belbachir and Makhoukhi, 2017; Gottlieb et al., 2003). Therefore, the discharge of dyes in wastewater, even in a small amount, is unpleasant and should be removed before they enter the environment. In this context, several treatment processes, including coagulation-flocculation (Renault et al., 2009), photocatalysis (Akhsassi et al., 2021; Fahoul et al., 2022; Mimouni et al., 2021; Naciri et al., 2021), ion exchange (Hassan and Carr, 2018), membrane filtration, and adsorption (Amjlef et al., 2021; Imgharn et al., 2021; Njoya et al., 2020) have been implemented to clean up colored effluents. Adsorption is considered an effective, green, and low-cost approach used for dye elimination from aqueous solutions. Therefore, the last decades have witnessed a huge interest in the development of efficient adsorbent materials. The performance of adsorbents depends on their physicochemical characteristics like porosity, particle size, surface functional groups, and chemical stability (Benjelloun et al., 2021; Laabd et al., 2021).

π-Conjugated polymers including polyaniline (PANI), polythiophene (PTh), and polypyrrole (PPy) have been widely employed in many fields like gas sensors, tissue engineering, photovoltaic cells, batteries, and wastewater purification (Liao et al., 2019). PANI is considered as the most promising conductive polymer among these polymers due to its particular characteristics: good redox reversibility, low-cost, environmental friendliness, excellent stability, good conductivity, and easy synthesis (Laabd et al., 2017;

Naciri et al., 2022). In addition, the uptake of organic dyes and heavy metal ions by PANI is high. The ion exchange property, porous structure as well as the presence of a large amount of protonated amine and imine groups on the surface of PANI are the reasons for its high adsorption capacity. However, the small particle size and poor physical (mechanical and thermal) properties of PANI seriously hinder its use in large scale wastewater purification systems (Sahu et al., 2019). In order to counterbalance these limitations, PANI-based composites using different reinforcing substrates like mineral clays (Zhou et al., 2017), natural lignocellulosic wastes (Kumar et al., 2008), activated carbon (Ansari et al., 2017) and zeolites (Abdellaoui et al., 2020; Shyaa et al., 2015) have been developed.

Zeolite has a tridimensional form of crystalline aluminosilicate, an open anionic framework consisting of tetrahedral oxygen-sharing TO_4, in which AlO_4 and SiO_4 are covalently linked to each other (Ba Mohammed et al., 2020; Shyaa et al., 2015). Besides, the zeolitic materials are microporous with a uniform pore distribution. As evidenced from the literature, the properties of zeolites can be enhanced by integrating different metals into their matrices. Incorporation of iron into adsorbents is highly preferred due to its economic, eco-friendly and semiconducting properties (Saifuddin et al., 2019). Several works focused on the optimization of the adsorption parameters and discussed the physical aspects of the process. However, only a restricted number of studies are available which decipher the main role of the active metal ions of the zeolite structure in the adsorption phenomenon.

Herein, we synthesized PANI@Fe-ZSM-5 zeolite hybrid composite through an oxidative polymerization route and characterized by SEM coupled with EDS, XRD, FTIR and XPS

analysis. The initial Orange G (OG) concentration, dosage of adsorbent, contact time, initial pH value of the solution and temperature were optimized to evaluate the effectiveness of the synthesized PANI@Fe-ZSM-5 composite for OG removal. The modeling of the equilibrium isotherms and adsorption kinetics of the OG dye on the composite was also evaluated. Furthermore, the theoretical predication of the OG molecules' binding on the surface of PANI@Fe-ZSM-5 was calculated using advanced statistical physics applied to the adsorption equilibrium. In addition, the effect of co-existing ions was assessed. Finally, the regeneration of PANI@Fe-ZSM-5 composite was performed to evaluate its reusability for OG dyestuff removal.

2. Experimental

2.1. Chemicals

Aniline monomer (Sigma-Aldrich) was used after distillation. Sodium persulfate ($Na_2S_2O_8$), acetone, ethanol, tetrapropylammonium bromide ($C_{12}H_{28}NBr$, 98 %), iron (III) nitrate pentahydrate ($Fe(NO_3)_3{\cdot}5H_2O$, ≥99.95 %), sulfuric acid (H_2SO_4, ≥95 %), sodium metasilicate (Na_2SiO_3, ≥98 %), hydrochloric acid (HCl, 37 %), sodium hydroxide (NaOH, ≥97 %), sodium chloride (NaCl, ≥99 %), and orange G (OG) dye were of analytical grade and purchased from Sigma-Aldrich. The dye solution was prepared by dissolving the accurately weighted dye in distilled water.

2.2. Preparation of Fe-ZSM-5 zeolite

The Fe-ZSM-5 zeolite synthesis was conducted using the procedure reported by Ba Mohammed et al. (Ba Mohammed et al., 2020). Briefly, 10 g of sodium metasilicate as a silicon precursor were dissolved in 25 mL of distilled water, and then 2 g of tetrapropylammonium bromide were added to the suspension under magnetic stirring

until the solution became uniform with a pH value of 10. The obtained solution was called first solution. A second solution was produced by dissolving 1 g of ferric nitrate pentahydrate in 10 mL of distilled water; then, the resulting solution was acidified using 2 ml of H_2SO_4 (0.01 M). This solution was poured dropwise into the first one and kept under stirring for 2 h. The formed gel was placed in a Teflon autoclave at 180 °C for 48 h. The resulting suspension was filtered and washed several times with acetone and distilled water. Finally, the as-prepared material was kept at 100 °C overnight to dry then calcined at 550 °C for 6 h.

2.3. Elaboration of PANI@Fe-ZSM-5

The PANI@Fe-ZSM-5 hybrid composite was prepared via an *in situ* oxidative polymerization of aniline with Fe-ZSM-5 particles in an acidic medium using $Na_2S_2O_8$ as oxidant, according to the procedure in (Hsini et al., 2021b): 1g of Fe-ZSM-5 was dispersed in 100 mL of a hydrochloric acid solution (1M) under stirring for 6 h. Then, 0.5 mL of aniline was added to the suspension under stirring for 3 h. A 50 mL solution of HCl (1 M) containing sodium persulfate (with a 0.5 monomer/oxidant molar ratio) was added dropwise into the mixture under agitation. A green suspension was obtained after 12 h, indicating the formation of doped PANI on the Fe-ZSM-5 particles. The resulting precipitate was filtered and washed with distilled water and acetone. The PANI@Fe-ZSM-5 composite was dried at 70 °C overnight.

2.4. Characterization of the adsorbent

To check out the hybrid composite crystal structure, X-ray powder diffraction (XRD) analyses were carried out with a BRUKER D8 ADVANCE TWIN diffractometer. The Fe-ZSM-5 surface morphology before and after polymerization was systematically

characterized by scanning electron microscopy (SEM) coupled with energy dispersive X-ray spectrometry (EDS) analysis (SEM, JEOL, JSM-IT200). X-ray photoelectron spectroscopy (XPS) analysis of the as-prepared PANI@Fe-ZSM5 composite was acquired using an ESCALAB 220 XL spectrometer equipped with a monochromatic Al Kα X-ray radiation source at 1486.6 eV. The binding energies were calibrated to the C1s peak at 284.6 eV. Fourier-transform infrared (FTIR) spectra of the obtained materials were acquired using KBr pellets using FTIR spectroscopy (ALPHA-Bruker Optics, Germany) in a wavenumber ranging from 400 to 4000 cm^{-1}.

The zero charge point (PZC) of the PANI@Fe-ZSM-5 composite was determined via potentiometric titration method reported by Fiol and Villaescusa (Fiol and Villaescusa, 2009). In short, 0.025 g of PANI@Fe-ZSM-5 was added to 50 mL of KNO_3 (0.03 M) solution and the pH of the solution was adjusted from 2 to 12 by adding HCl (0.1 M) or NaOH (0.1 M) aqueous solutions. The mixtures were stirred for 24 h at ambient temperature. The final pH_f of each solution was assessed. Then, the PZC was identified as pH_i when ΔpH is zero.

2.5. Adsorption experiments and regeneration

The OG dye adsorption onto PANI@Fe-ZSM-5 hybrid composite was conducted in a batch reactor under various operational conditions. To evaluate the effect of adsorbent dose, various amounts of PANI@Fe-ZSM-5 composite (0.2-2 g/L) were introduced into 50 mL of OG dye solution at 20 mg/L initial concentration for 180 min at pH 6.0 and 25 °C. The influence of pH on the OG dye removal efficiency was studied by changing the solution pH from 2 to 12 with an adsorbent dose of 0.5 g/L. Under the same experimental conditions, the influence of initial concentration of OG dye (from 20 to 500 mg/L), contact time and

temperature was also assessed. After adsorption, the adsorbent was removed from adsorbate solution by filtration on Millipore filters (0.45 μm). The equilibrium concentration of OG dye was quantified by UV2300 spectrophotometer at 476 nm.

The ~~absorbed~~ percentage R(%) and the adsorption capacity Q_e(mg/g) were calculated by the following relations (Ait Haki et al., 2021; Brini et al., 2021b):

$$R\% = \frac{(C_0 - C_e)}{C_0} \times 100 \quad (1)$$

$$Q_e = \frac{(C_0 - C_e).V}{m} \quad (2)$$

Where C_o (mg/L) is the initial OG concentration, C_e (mg/L) is the OG concentration at equilibrium, m (g) is the mass of the PANI@Fe-ZSM-5 composite, and V (L) is the volume of the solution.

In order to bring up the adsorption process more economically reliable and eco-friendly, the regeneration of PANI@Fe-ZSM-5 composite after the adsorption experiment is a very important aspect. For desorption/adsorption study, 0.3 g of PANI@Fe-ZSM-5 was introduced in 0.6 L of 20 mg/L OG dye solution. After 180 min of sorption, desorption experiment was performed using 0.5 M NaOH as eluent solution for 6 h. After that, the regenerated PANI@Fe-ZSM-5 composite was washed with distilled water, and then redoped with 1 M HCl solution. The fresh PANI@Fe-ZSM-5 composite was used for a subsequent OG adsorption cycle. In this work, five regeneration cycles were carried out.

2.6. Theoretical background

The statistical physics theory is an emerging effective approach to deeply illuminate the adsorption mechanisms at the liquid-solid interface (Mobarak et al., 2019b, 2019a;

Mohamed et al., 2020). The adsorption performance of OG dye on the PANI@Fe-ZSM-5 hybrid composite was examined by applying five statistical physics models to the experimental equilibrium data.

- First model (**M1**): Monolayer model with similar receptor sites. This model assumes that the adsorption process occurs by the formation of a monolayer on the adsorbent surface with one type of adsorption sites (Mobarak et al., 2019b, 2019a). The analytical expression of the M1 model is given by Eq. (3):

$$Q_e = nN_o = \frac{nN_M}{1+\left(\frac{C_{1/2}}{C_e}\right)^n} = \frac{Q_{sat}}{1+\left(\frac{C_{1/2}}{C_e}\right)^n} \quad (3)$$

where Q_e (mg/g) and C_e (mg/L) denote the equilibrium adsorbed amount and equilibrium concentration, respectively; n represents the number of adsorbed molecules per binding site; N_M (mg/g) is the active sites density; Q_{sat} (mg/g) is the adsorption capacity at saturation; $C_{1/2}$ (mg/L) is the adsorbate concentration at half-saturation.

- Second model (**M2**): Double-layer model with similar receptor sites. This model is appropriate to describe the double-layer adsorption process over the adsorbent surface with identical binding sites. The formalism of the M2 model is presented by Eq. (4):

$$Q_e = nN_M \frac{\left(\frac{C_e}{C_{1/2}}\right)^n + 2\left(\frac{C_e}{C_{1/2}}\right)^{2n}}{1+\left(\frac{C_e}{C_{1/2}}\right)^n + \left(\frac{C_e}{C_{1/2}}\right)^{2n}} \quad (4)$$

- Third model (**M3**): Monolayer model with two different energies. This model is established on the hypothesis that the adsorption process is a monolayer coverage over two kinds of adsorbent active sites (with different energies) (Mobarak et al., 2019b, 2019a).

$$Q_e = \frac{n_1 N_{1M}}{1+(C_1/C_e)^{n_1}} + \frac{n_2 N_{2M}}{1+(C_2/C_e)^{n_2}} \qquad (5)$$

where $\mathbf{C_1}$ and $\mathbf{C_2}$ (mg/L) are the half-saturation concentrations for the first and the second adsorption sites, respectively; $\mathbf{N_{1M}}$ and $\mathbf{N_{2M}}$ (mg/g) are the receptor site densities of the first and the second kinds of active sites, respectively; $\mathbf{n_1}$ and $\mathbf{n_2}$ are the number of adsorbed molecules by each binding site for the first and the second kinds of active sites, respectively.

- Fourth model (**M4**): Double-layer model with two different energies. This model is suitable to predict the double-layer adsorption on the two different types of adsorbent active sites. The equation of the M4 model is given as:

$$Q_e = nN_M \frac{\left(\frac{C}{C_1}\right)^n + 2\left(\frac{C}{C_2}\right)^{2n}}{1+\left(\frac{C}{C_1}\right)^n + \left(\frac{C}{C_2}\right)^{2n}} \qquad (6)$$

where **C** (mg/L) denotes the equilibrium concentration; $\mathbf{N_M}$ (mg/g) refers to receptor sites density; $\mathbf{C_1}$ and $\mathbf{C_2}$(mg/L) correspond to the concentrations at half-saturation for the first and the second type of active sites, respectively.

- Fifth model (**M5**): Finite multi-layer model. This model suggests the occurrence of multilayer adsorption process. The formalism of the M5 model is expressed as follows:

$$Q_e = nN_M \frac{\left(\frac{C}{C_1}\right)^n \left(1-(N_\ell+1)\left[\frac{C}{C_2}\right]^{nN_\ell} + N_\ell\left[\frac{C}{C_2}\right]^{n(N_\ell+1)}\right)}{\left(1-\left[\frac{C}{C_2}\right]^n\right)\left(1-\left[\frac{C}{C_2}\right]^n + \left[\frac{C}{C_1}\right]^n - \left[\frac{C}{C_1}\right]^n\left[\frac{C}{C_2}\right]^{nN_\ell}\right)} \qquad (7)$$

where $\mathbf{(N_l + 1)}$ represents the number of adsorption layers; **n** refers to the number of ions per adsorption site; $\mathbf{N_M}$ (mg/g) refers to receptor sites density; $\mathbf{C_1}$ and $\mathbf{C_2}$(mg/L)

correspond to the concentrations at half-saturation for the first and the second type of active sites, respectively.

The equations of the above-presented statistical physics models were derived from the corresponding grand-canonical partition functions in the statistical physics (Mobarak et al., 2019b, 2019a). These models were fitted to the experimental results of OG dye adsorption onto PANI@Fe-ZSM-5 composite using Mathematica 11 program. The appropriateness of the selected models was evaluated based on the correlation coefficient (R^2) and root mean squared error (RMSE) values (Mobarak et al., 2019b).

$$RMSE = \sqrt{\frac{\sum_{i=1}^{m}(Q_{i\,cal}-Q_{i\,exp})^2}{p-q}} \qquad (8)$$

where $\boldsymbol{p}$ and $\boldsymbol{q}$ represent the number of actual data and adjustable parameters, respectively. $\boldsymbol{Q_{i\,cal}}$ and $\boldsymbol{Q_{i\,exp}}$ denote the computed and the experimental OG dye uptake capacities, respectively.

3. Results and discussion

3.1. Surface characterization and XRD analysis

Fig. 1 depicts the morphology and elemental analysis of Fe-ZSM-5 particles before and after the polymerization of aniline. According to **Fig. 1(a)**, the SEM image of Fe-ZSM-5 features smooth agglomerated spheres with a size ranging from 1 to 5 μm. **Fig. 1(b)** confirms the deposition of polyaniline onto the Fe-ZSM-5 surface with a flake-like structure. This surface morphology may constitute a good platform for the removal of pollutants from aqueous media. In addition, the acquired textural information reveals good adhesion of PANI onto the Fe-ZSM-5 surface. This may be due to interactions

241 (hydrogen bonds) between the amine groups of aniline and the hydroxyl groups (Si-OH)
242 of the Fe-ZSM-5 zeolite (Ba Mohammed et al., 2020). From **Figs. 1(c)** and **(d)**, the
243 elemental analysis of the Fe-ZSM-5 zeolite by EDS proves the existence of the following
244 elements: oxygen (50.51%), silicon (41.98%), iron (5.23%) and sodium (2.28%). This
245 result indicates that silicon oxide (SiO_2) is the major phase of the Fe-ZSM-5 zeolite. After
246 the polymerization of aniline on the surface of Fe-ZSM-5 zeolite, the EDS spectrum shows
247 the appearance of carbon (38.06%). In addition, the EDS spectrum of PANI@Fe-ZSM-5
248 features other characteristic elements (N, Cl and S), which affirms that the surface of Fe-
249 ZSM-5 is well-coated by PANI.

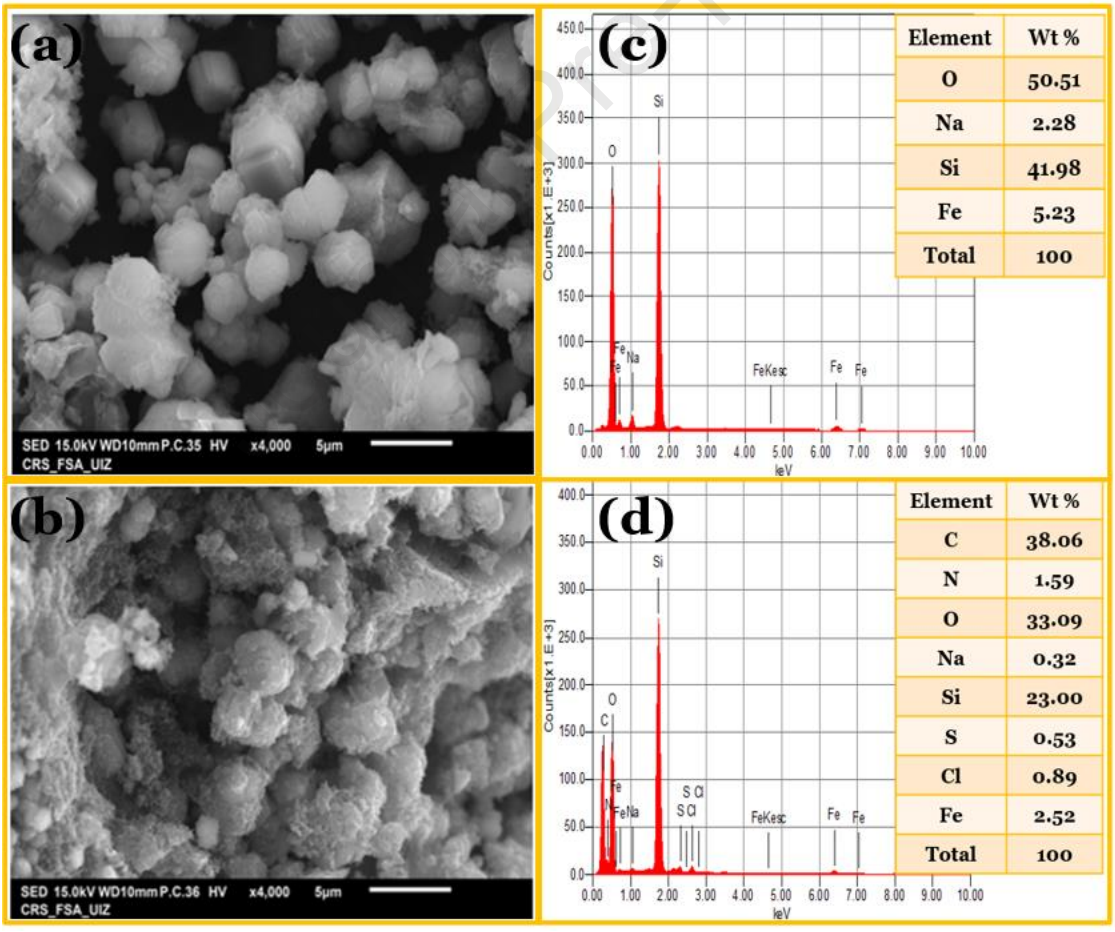

250

Fig. 1. (a) SEM micrographs of Fe-ZSM-5, **(b)** PANI@Fe-ZSM-5 and **(c and d)** their respective EDS elemental spectra.

X-ray diffraction is an important technique used to identify the crystalline phases and structural properties of solid materials. Therefore, the as-prepared Fe-ZSM-5 zeolite and PANI@Fe-ZSM-5 composite were analyzed by this technique and the obtained XRD patterns are displayed in **Fig. 2(a)**. The synthesized Fe-ZSM-5 zeolite sample exhibited peaks at 2θ=7.95°, 8.80°, 23.10°, 23.94° and 24.40° associated with [0 1 1], [0 2 0], [0 5 1], [0 3 3] and [3 1 3] planes, with corresponding d-spacing values of 1.11, 1.00, 0.38, 0.37 and 0.36 nm, respectively. These values are in good agreement with the peaks of Fe-ZSM-5 zeolite (JCPDS no. 43-0321) with a well-resolved mordenite framework inverted (MFI) structure (Chemical formula: $H_{0.32}Al_{0.32}Si_{95.68}O_{192}$, Crystal system: Monoclinic and Space group: P21/n) (Narayanan et al., 2015). Moreover, the sharpness of the peaks of the diffraction peaks suggests that the as-prepared Fe-ZSM-5 sample has a more crystalline nature and no other peaks appeared, which discloses that the as-prepared Fe-ZSM-5 material does not contain any impurities (Liu et al., 2011). Compared with bare Fe-ZSM-5 sample, the peak intensities of the [0 1 1] and [0 2 0] planes of PANI@Fe-ZSM-5 composite were markedly decreased due to the PANI coating on the Fe-ZSM-5 surface, but their crystal framework structure was preserved. Moreover, no characteristic diffraction peaks of PANI were detected in PANI@ZSM-5 composite, because PANI was in amorphous phase. Furthermore, the absence of impurity phases in the XRD curves indicates the successful synthesis of PANI@Fe-ZSM-5 composite.

3.2. FTIR data analysis

The FTIR spectrum of Fe-ZSM-5 and PANI@Fe-ZSM-5 are depicted in **Fig. 2(b)**. The FTIR spectrum of Fe-ZSM-5 exhibits a characteristic peak at about 3854 cm^{-1} ascribed to the silanol groups ~~of~~ Si–OH. The absorption bands at 2915 and 2840 cm^{-1} can be assigned to the residual methyl ($–CH_3$) and methylene ($–CH_2$) vibrations of tetrapropylammonium bromide precursor (Kachangoon et al., 2020). The peak located at 1631 cm^{-1} is ascribed to the stretching bending of adsorbed water molecules. The symmetric stretching of external linkages of the tetrahedron appears at around 792 cm^{-1} (Liu et al., 2011). Also, the spectrum comprises a peak at 556 cm^{-1} assigned to the stretching vibrations of Fe–O of Fe_2O_3 (Suresh et al., 2014). The peaks at 477 and 1220 cm^{-1} are attributed to the Si–O bending vibrations of SiO_4 internal tetrahedral (Doula, 2007), (Niu et al., 2017). The FTIR spectrum of PANI@Fe-ZSM-5 reveals the appearance of a new peak at 3520 cm^{-1} assigned to the N–H stretching vibration, indicating the existence of amine groups. Besides, the vibration bands at 1580 and 1440 cm^{-1} are ascribed to the stretching vibration ~~C=C~~ in quinoid and benzenoid structure of doped PANI, respectively (Xu et al., 2014). These findings confirm that the PANI was well-incorporated onto the surface of Fe-ZSM-5 particles.

3.3. XPS analysis

XPS analysis was performed to assess the chemical composition and ~~chemical~~ state of the PANI@Fe-ZSM5 surface. The full survey XPS survey of PANI@Fe-ZSM5 composite is depicted in **Fig. 2(c)**. The spectrum revealed the presence of O_{1s} (531.5 eV), N_{1s} (397.9 eV) and C_{1s} (283.6 eV) as the main components of the PANI@Fe-ZSM5 surface (Abdel Hamid et al., 2019). Besides, the presence of three weak peaks confirmed the occurrence of silicon (Si2p and Si2s at 101.9 and 152.6 eV, respectively), sulfur (S_{2p} at 168.1 eV) and chlorine

296 (Cl_{2p} at 199.4 eV) elements on the PANI@Fe-ZSM-5 surface (Abdel Hamid et al., 2019;
297 Ravelo-Acuña et al., 2019; Zhang et al., 2016). The Si element is related to the silica in the
298 ZSM-5 zeolite. The other elements (e.g., Fe and Al) of Fe-ZSM-5 zeolite were not detected,
299 which eventually due to the formation of thick PANI layer on the surface of Fe-ZSM-5
300 zeolite (penetration depth of the X-ray beam does not exceed 10 nm). The Cl and S
301 elements are indicative of the existence of chloride anion doping (Cl^-) and oxidizing agent
302 (sodium persulfate) on the PANI@Fe-ZSM-5 surface. From **Fig. 2(d)**, the C_{1s} high
303 resolution spectrum was fitted with three peaks located at 284.9 (C–C/C–H), 285.7 (C–
304 N/C=N) and 287.1 eV ($C–N^+/C=N^+$) (Chan et al., 1992; Wang et al., 2015). The positively
305 charged N-containing functional groups indicated the doping of PANI chains by sulfate
306 and chloride ions generated from the oxidant and HCl acid (Wang et al., 2005). **Fig. 2(e)**
307 shows that the N1s spectrum ~~which~~ can be deconvoluted into two peaks at 398.4 and 399.6
308 eV ascribed to amine (–NH–) and doped quinonoid imine ($–NH^+=$) of benzenoid ring,
309 respectively (Bhaumik et al., 2021). The XPS results demonstrated that the PANI
310 Emeraldine salt (doped form) was successfully coated on the Fe-ZSM-5 zeolite.

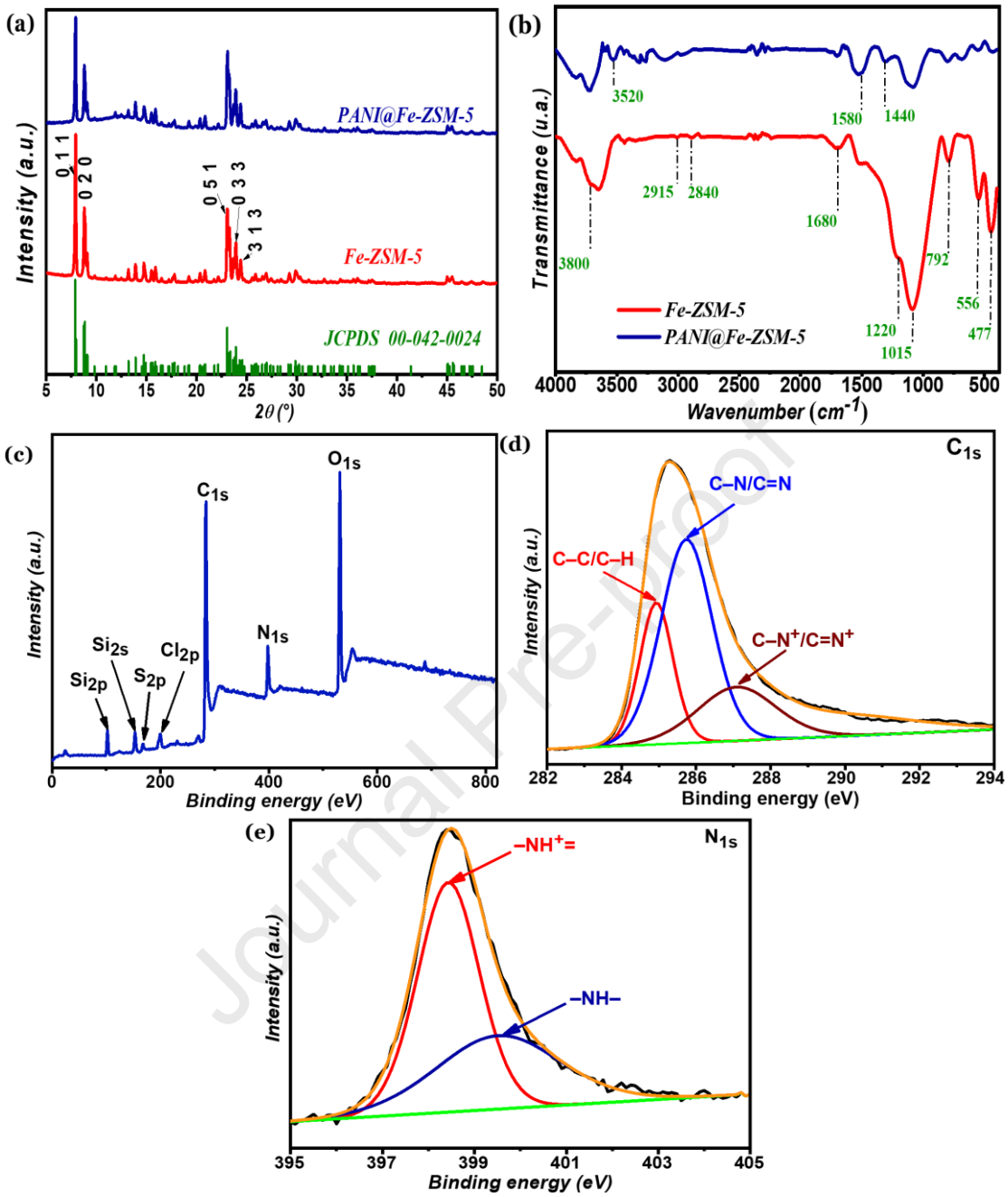

311

312 **Fig.2. (a)** XRD patterns of Fe-ZSM-5 and PANI@Fe-ZSM-5 composite; **(b)** FTIR

313 spectra of Fe-ZSM-5 zeolite and PANI@Fe-ZSM-5 composite; **(c)** XPS wide scan

314 spectrum; **(d)** C_{1s} and **(e)** N_{1s} core level spectra of the PANI@Fe-ZSM-5 composite.

315

3.4. Adsorption study

3.4.1. Effects of adsorbent dosage and pH

The influence of sorbent dosage on the OG dye adsorption was investigated in the 0.2 to 2.0 g/L concentration range. **Fig. 3(a)** displays the removal efficiency and uptake capacity of OG onto PANI@Fe-ZSM-5 at different adsorbent doses. The adsorption percentage was increased up to 96.37 % with the increase of PANI@Fe-ZSM-5 dose from 0.2 to 0.5 g/L. This might be due to the increment in the number of adsorbate binding sites available for OG dye removing (Hsini et al., 2020). Increasing the PANI@Fe-ZSM-5 dosage beyond 0.5 g/L did not affect the OG dye adsorption efficiency. This trend may be due to the exhaustion of OG dye molecules. Besides, the uptake capacity was decreased, owing to the formation of adsorbent particles aggregates, which could minimize the availability of surface sites for OG dye adsorption (Hsini et al., 2021d; Tu et al., 2020).

It is widely-~~known~~ that the solution pH is a key operating condition in adsorption processes (Hsini et al., 2021a). The surface charge of the PANI@Fe-ZSM-5 composite was investigated as a function of pH (inset of **Fig. 3(b)**). The PZC value of PANI@Fe-ZSM-5 composite was found to be 3.75. This means that the as-prepared PANI@Fe-ZSM-5 material surface is positively charged at pH below 3.75, while the surface becomes negatively charged at pH above 3.75. The influence of the solution pH on the adsorption process over the pH range 2–12 is displayed in **Fig. 3(b)**. As a result, the maximum removal percentage of OG dye was achieved at low pH values. That could be elucidated by the protonation of adsorbent sites (protonated silanol and amine groups), which results in the increment of the electrostatic interactions between anionic OG dye and positively charged PANI@Fe-ZSM-5 surface (Ba Mohammed et al., 2020). Whilst, at higher pH, the

OG dye adsorption efficiency decreased due to a decline of the number of positively charged sites. Therefore, we can conclude that the adsorption of OG dye on the as-prepared adsorbent surface is executed through electrostatic interactions (Yeamin et al., 2021), as well as the involvement of π-π ones (Nasar and Mashkoor, 2019). Besides, under alkaline conditions, the competitive adsorption of OH^- ions with OG anions could be another reason to explain the observed downward trend of OG dye removal efficiency. In the next adsorption experiments, the pH value of OG solutions was maintained at 6.0 to minimize the costs related to the pH adjustment. It is worth highlighting the pivotal role of electrostatic and π-π interactions in the OG dye adsorption mechanism. Based on the above discussion, a binding mechanism of OG dye on the PANI@Fe-ZSM-5 surface is proposed in **Fig. 6(d)**. To further confirm the adsorption of OG dye, the adsorbent surface after adsorption was analyzed by the FTIR technique. The FTIR spectra of PANI@Fe-ZSM-5 before and after OG dye removal are depicted in **Fig. 6(c)**. As a result, the FTIR data showed that there is no obvious shift in the bands of the functional groups on the PANI@Fe-ZSM-5 surface after adsorption, indicating that the molecular structure of the PANI@Fe-ZSM-5 composite remained unaltered after OG dye removal. Furthermore, no new peak was observed after OG adsorption, suggesting that there is no chemical interaction of OG molecules with PANI@Fe-ZSM-5. Therefore, it can be concluded that the binding of OG dye molecule on the PANI@Fe-ZSM-5 surface sites takes place via physical interactions (e.g., electrostatic forces and π-π interactions). In light of the above presented discussion, a graphical illustration of the proposed adsorption mechanism is presented in **Fig. 6(d)**.

3.4.2. Adsorption kinetics

The result of adsorbent/adsorbate contact time on the removal of OG dye by PANI@Fe-ZSM-5 composite surface was investigated by plotting the adsorption capacity of OG dye versus contact time (from 2 to 180 min). The adsorbent dosage of 0.5 g/L was used in 100 mL of OG solution with 20 mg/L initial concentration at pH 6 and 25 ◦C. From **Fig. 3(c)**, it can be seen that upon increasing the contact time, the OG dye uptake was improved. In the first 60 min, the increase was rapid then it became slow, and the equilibrium was reached after 120 min. Thus, the removal ability of PANI@Fe-ZSM-5 composite was related to the binding sites availability on the PANI@Fe-ZSM-5 surface for OG textile dye removal (Tu et al., 2020). The pseudo-first-order, pseudo-second-order, and intra-particle diffusion kinetic models were used to fit the kinetic data to evaluate the kinetic mechanism of OG adsorption on the PANI@Fe-ZSM-5 composite (Abbasi, 2017). The nonlinear equations and the corresponding fitting parameters of pseudo-first-order and pseudo-second-order kinetic models are summated in **Table S1** and **Fig. 3(c).** As shown in **Fig. 3(c)**, the pseudo-second-order model with R^2 of 0.97 is the model which had the highest correlation coefficient than the pseudo-first-order model (0.91). Furthermore, the adsorption capacity, calculated from pseudo-second-order model (37.99 mg/g), was found to be close to the experimentally-determined one (37.15 mg/g), confirming that the OG dye adsorption process was better described by this kinetic model.

In order to investigate the mass transfer mechanism that occurred during the adsorption process, the intraparticle diffusion model was applied to the actual removal data (Tang and Zhang, 2016). The fitting parameters are listed in **Table S1**. **Fig. 3(d)** illustrated that the removal of OG dye by the PANI@Fe-ZSM-5 composite consisted in three successive

stages. The first one was ascribed to the diffusion of OG dye molecules from the aqueous phase to the external surface sites of as-prepared composite. The second stage implicates the intra-particle diffusion as rate-controlling step. In the last stage the intraparticle diffusion rate decreased, because of the extremely low concentration of OG (Tang and Zhang, 2016). Besides, these results were supported by the reduction of rate constant values when going from the first stage to the last one.

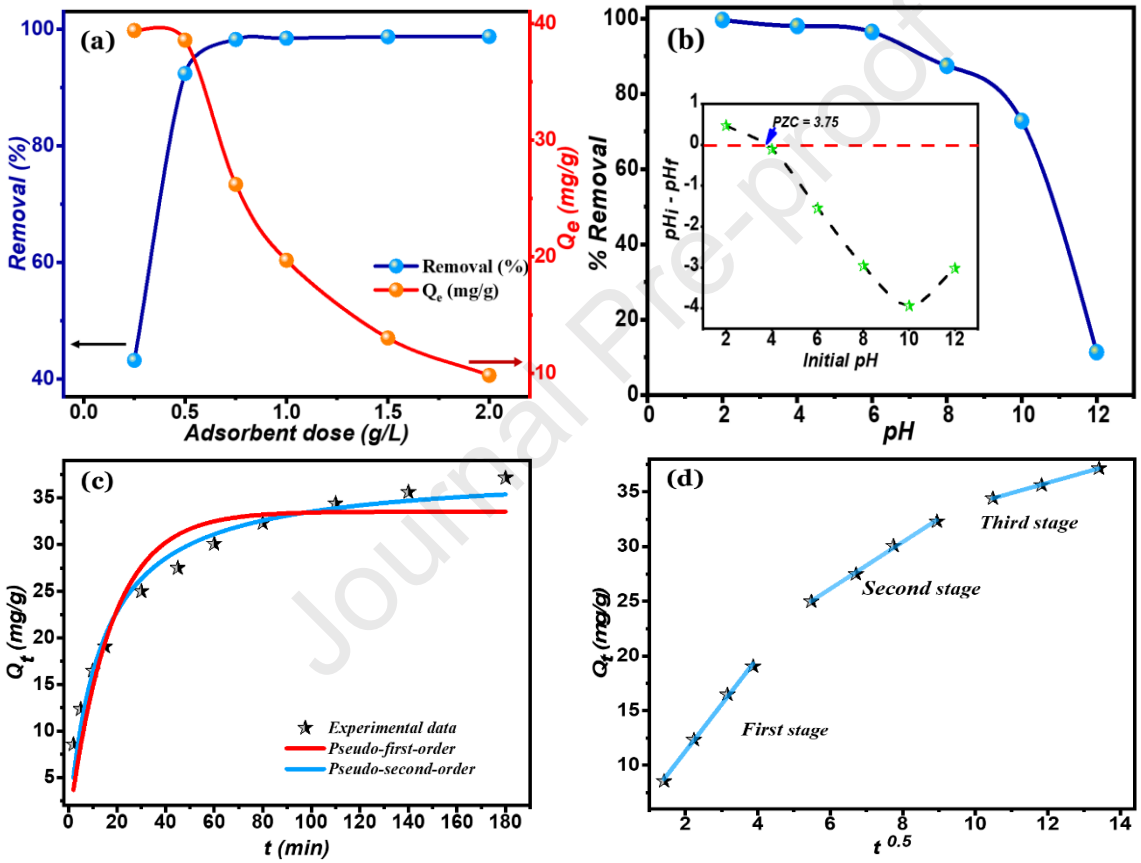

Fig. 3. **(a)** Effect of PANI@Fe-ZSM-5 dose on the OG dye adsorption efficiency (Conditions: equilibrium time = 180 min; OG dye concentration = 20 mg/L; temperature = 25 ◦C); **(b)** Adsorption efficiency of the OG dye onto PANI@Fe-ZSM-5 at different pH values (inset: PZC determination of the PANI@Fe-ZSM-5 composite), **(c)** Pseudo-first-order and pseudo-second-order kinetics models; **(d)** intraparticle diffusion model.

3.5. Advanced statistical physics interpretation

The fitting of the considered statistical physics models to the experimental data for OG dye removal by the PANI@Fe-ZSM-5 composite was evaluated based on the determination of R^2 coefficient and RMSE values. From **Table S2**, it is clear that the **M3** model (monolayer model with two different energies) demonstrated good correlation with OG dye adsorption data (high R^2 values and low RMSE values) for all tested temperatures (**Fig. 4(a)**). Therefore, the **M3** model was chosen as the best fitting statistical physics model to elucidate the macroscopic and microscopic properties of the OG dye removal process by the PANI@Fe-ZSM-5 composite.

3.5.1. *Statistical physics parameters*

To shed light on the orientation of OG dye molecules on the PANI@Fe-ZSM-5 surface, the values of the stoichiometric coefficient (n) were calculated at different temperatures (**Fig. 4(b) and Table S3**). On the one hand, n_1 values (for the first type of active sites) are less than 1, indicating that the OG dye molecules adsorbed parallelly on the first type of active surface sites of PANI@Fe-ZSM-5 composite. In addition, each receptor site (first type) of PANI@Fe-ZSM-5 composite adsorbs more than one OG dye molecule, suggesting a multi-docking adsorption mechanism (Sellaoui et al., 2015). This adsorption behavior becomes more pronounced with increasing temperature (n_1 values decreased). On the other hand, the n_2 values (for the second type of active sites) are superior to unity, revealing that the OG dye molecules adsorbed perpendicularly *via* a multimolecular mechanism on the second type of active sites of PANI@Fe-ZSM-5 composite (Laabd et al., 2022). Moreover, it is worth noticing that the n_2 values increased with the increase of temperature,

highlighting that the thermal agitation results in the decrease in the aggregation of the OG dye molecules in the liquid phase (Li et al., 2019).

The density of active sites (N_M) is a crucial parameter governing the removal performance. The temperature dependence of N_M parameter for OG dye removal by PANI@Fe-ZSM-5 composite surface is presented in **Fig. 4(c)**. It can be observed that the N_{1M} (for the first type of active sites) and N_{2M} (for the second type of active sites) parameters follow an inverse trend compared to n_1 and n_2 stoichiometric coefficients, respectively. This result could be attributed to steric-hindrance effect of OG dye molecules during the adsorption process onto the PANI@Fe-ZSM-5 surface (Sellaoui et al., 2017b). Indeed, as the number of adsorbed OG dye molecules per active site (n) decreases, the number of available adsorption sites increases, thus leading to an increase in the density of active sites (N_M), and vice versa.

The saturation uptake capacity (Q_{sat} in mg/g) of the PANI@Fe-ZSM-5 composite for OG dye adsorption depends on the stoichiometric coefficient (n) and density of active sites ($Q_{sat} = nN_M$). From **Fig. 4(d)**, it is convenient to mention that the adsorbed amounts (Q_1 and Q_2) increased with raising the temperature (endothermic process), confirming that the total OG dye adsorption capacity (Q_{sat}) is predominantly affected by the density of active sites (N_M) rather than the stoichiometric coefficient (n).

From an energetic point of view, the removal of OG dye by the PANI@Fe-ZSM-5 composite was assessed by calculating the adsorption energies E1 and E2 for the first and second types of active sites, respectively. The values of E1 and E2 can be computed by the following Eqs.:

$$E_1 = \mathrm{RTln}\left(\frac{C_s}{C_1}\right) \quad (9)$$

$$E_2 = \mathrm{RTln}\left(\frac{C_s}{C_2}\right) \quad (10)$$

where Cs (mg/L) is the aqueous solubility of OG dye. C_1 and C_2 represent the half-saturation concentrations (mg/L) for the first and the second types of adsorption sites, respectively. R (8.314 J/mol K) is the universal gas constant and T is the temperature (K).

Fig. 4(e) shows the influence of temperature on the removal energy. It is noteworthy that the values of adsorption energies are positive and increased with temperature, proving that the OG dye removal by the PANI@Fe-ZSM-5 composite is an endothermic process. Therefore, the adsorption method is favorable at higher temperatures, which is in concordance with the saturation adsorption capacity. Moreover, the figure shows that E1 is higher than E2, which confirm that PANI@Fe-ZSM-5 has a higher interaction with OG dye. From the calculated values of adsorption energies, we deduce that the adsorption was a physical process since these values are <40 kJ/mol (Seliem and Mobarak, 2019). The adsorption ~~formed bonds could be a~~ hydrogen bonds or ~~Van~~ der Waals or dipole-dipole interactions (Wjihi et al., 2020, 2017), reinforcing that the OG dye adsorption is physisorption in nature (Sellaoui et al., 2016).

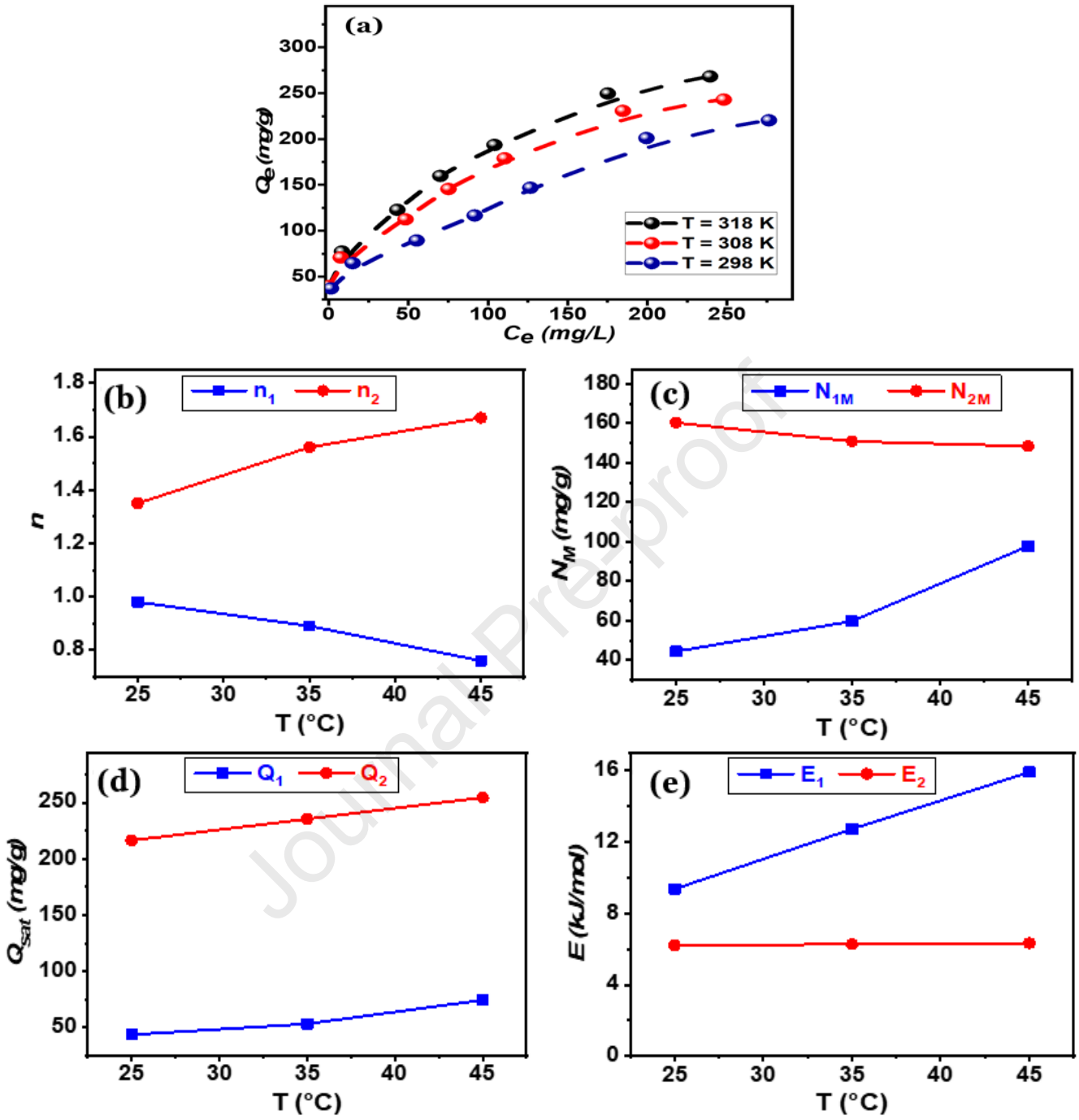

Fig. 4. (a) Fitting of actual equilibrium data of OG dye removal by the PANI@Fe-ZSM-5 composite to the M3 model (best fitted model); **(b)** The stoichiometric coefficient; **(c)** the density of active sites; **(d)** the saturation uptake capacity and **(e)** the adsorption energy for OG dye removal by the PANI@Fe-ZSM-5 composite at different temperatures.

3.5.2. *Thermodynamic functions*

The thermodynamic functions (entropy, free enthalpy and internal energy) related to the OG dye adsorption on the PANI@Fe-ZSM-5 composite were calculated using the monolayer ~~layer~~ model with the different energy sites (**M3**). The entropy function is of prime importance to predict the randomness of OG dye molecules at the solution-adsorbent interface. This thermodynamic function was calculated according to the following Eq. (Seliem and Mobarak, 2019):

$$\frac{S}{k_B} = \frac{-Q_{sat.1}\left[\frac{C}{C_1}\right]^{n_1}\ln\left[\frac{C}{C_1}\right]+Q_{sat.2}\left[\frac{C}{C_2}\right]^{n_2}\ln\left[\frac{C}{C_2}\right]+\left[\frac{C}{C_1}\right]^{n_1}\left[\frac{C}{C_2}\right]^{n_2}\left(Q_{sat.1}\ln\left[\frac{C}{C_1}\right]+Q_{sat.2}\ln\left[\frac{C}{C_2}\right]\right)}{\left(1+\left[\frac{C}{C_1}\right]^{n_1}\right)\left(1+\left[\frac{C}{C_2}\right]^{n_2}\right)+\ln\left(\left(1+\left[\frac{C}{C_1}\right]^{n_1}\right)^{N_{1M}}\left(1+\left[\frac{C}{C_2}\right]^{n_2}\right)^{N_{2M}}\right)} \quad (11)$$

To evaluate the spontaneity of the OG dye adsorption system, the free enthalpy function is computed as follows (Ayachi et al., 2019):

$$\frac{G}{k_B T} = \ln\left[\frac{\mu}{Z_{tr}}\right]\left(\frac{Q_{sat.1}}{1+\left[\frac{C_1}{C}\right]^{n_1}}+\frac{Q_{sat.2}}{1+\left[\frac{C_2}{C}\right]^{n_2}}\right) \quad (12)$$

The internal energy (E_{int}) represents the sum of energies in the adsorption system. This thermodynamic function is written as follows (Seliem and Mobarak, 2019):

$$\frac{E_{int}}{k_B T} = \frac{-N_{1M}\left[\frac{C}{C_1}\right]^{n_1}\left(n_1\ln\left[\frac{C}{C_1}\right]-\mu\right)+N_{2M}\left[\frac{C}{C_2}\right]^{n_2}\left(n_2\ln\left[\frac{C}{C_2}\right]-\mu\right)+\left[\frac{C}{C_1}\right]^{n_1}\left[\frac{C}{C_2}\right]^{n_2}\left(N_{1M}\left(n_1\ln\left[\frac{C}{C_1}\right]-\mu\right)+N_{2M}\left(n_2\ln\left[\frac{C}{C_2}\right]-\mu\right)\right)}{\left(1+\left[\frac{C}{C_1}\right]^{n_1}\right)\left(1+\left[\frac{C}{C_2}\right]^{n_2}\right)} \quad (13)$$

In Eqs. (11-13), k_B, μ and Z_{tr} are the Boltzmann constant, chemical potential and translation partition function, respectively.

The evolution of the entropy function during the OG dye adsorption versus equilibrium OG dye concentration at different temperatures (298, 308 and 318 K) is displayed in **Fig.**

5(a). From this figure, the entropy function exhibited similar trend for all studied temperatures. In addition, we can see that, with increasing the equilibrium OG dye concentration, the entropy of OG dye removal system increased until a maximum at the half-saturation concentration and then decreased. At lower OG dye concentrations, the OG molecules possessed high probability to select an active site on the PANI@Fe-ZSM-5 surface, resulting in an increase of disorder at the solution-adsorbent interface. At higher OG dye concentrations, the PANI@Fe-ZSM-5 surface tended to the saturation and the probability of OG molecules to find a vacant adsorption site was significantly decreased. Therefore, the entropy shifted towards lower values (decrease of disorder).

Fig. 5(b) represents the evolution of the free enthalpy as a function of OG dye concentration. As a result, the negative values of the free enthalpy function revealed that the OG adsorption on the PANI@Fe-ZSM-5 composite is a spontaneous process for all investigated temperatures (Sellaoui et al., 2016). Besides, it can be seen that the free enthalpy decreases with increasing temperature and OG dye concentration. Thus, we can conclude that the OG dye adsorption process is more favorable at higher temperatures (endothermic process) and higher OG dye concentrations (increase in the concentration gradient). **Fig. 5(c)** displays the variation of internal energy versus equilibrium OG concentration at different temperatures. The negative values of the internal energy during the OG dye adsorption on the PANI@Fe-ZSM-5 composite confirms its spontaneous nature (Sellaoui et al., 2017a), reflecting that the OG dye molecules exhibited good binding affinity with the PANI@Fe-ZSM-5 surface. Moreover, the internal energy tremendously decreases with OG concentration ~~at~~ low concentration range, which indicates that the OG dye molecules target the most active sites on the PANI@Fe-ZSM-5 surface. When the OG dye concentration is increased, the availability of PANI@Fe-ZSM-5 surface sites decreases

513 and the OG dye molecules interact with the less active sites, resulting in a slight
514 diminution in the internal energy (Khalfaoui et al., 2015).

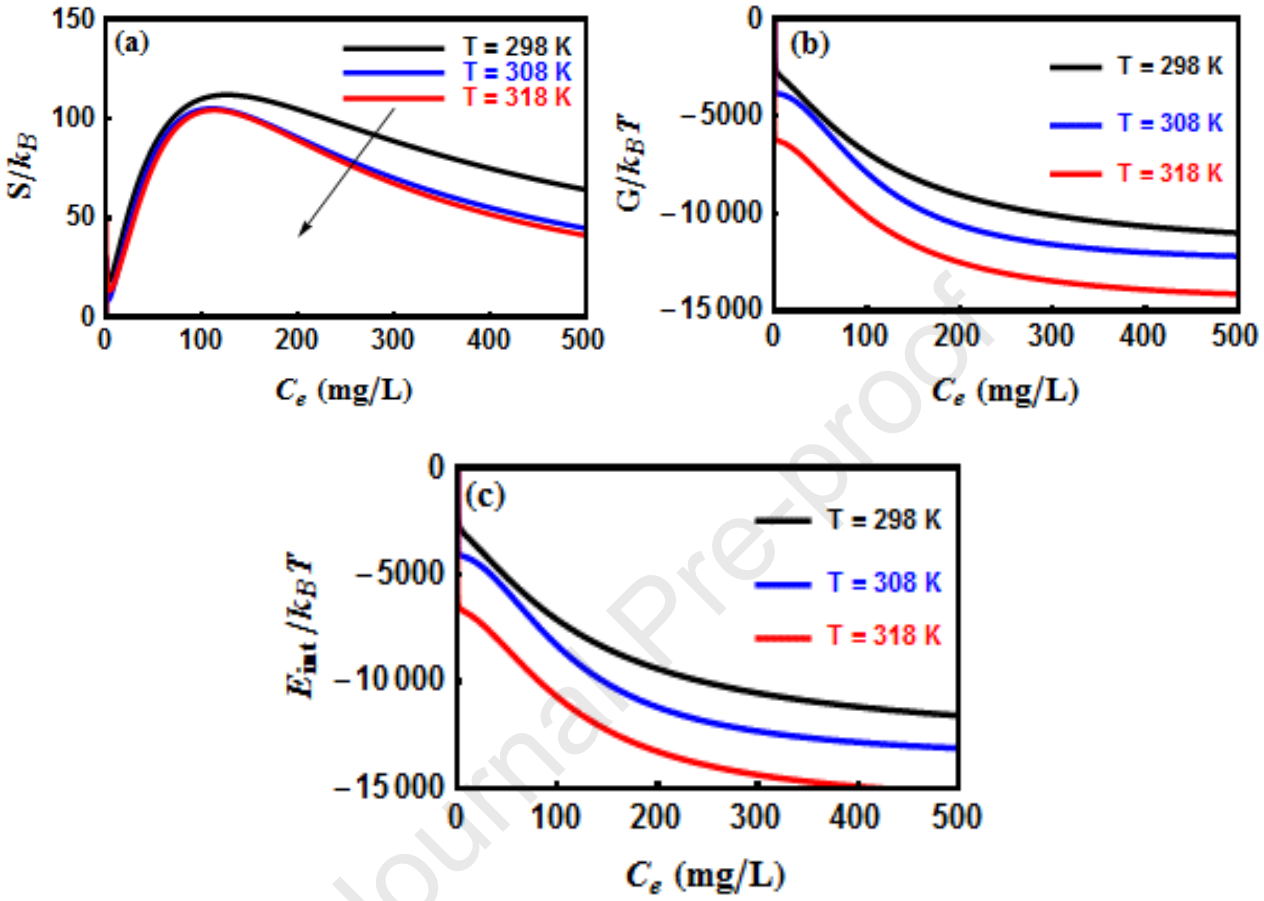

516

517 **Fig. 5.** Thermodynamic functions: **(a)** entropy; **(b)** free enthalpy and **(c)** internal
518 energy for OG dye adsorption on the PANI@Fe-ZSM-5 composite.

519 ### 3.6. Effect of co-existing ions and Regeneration

520 It has been known that the wastewaters are polluted not only by dyes, but also by other
521 organic and inorganic pollutants (Ansari et al., 2017). Thus, it is necessary to assess the
522 influence of coexisting ions. For this goal, a series of adsorption tests were carried out by
523 keeping the concentration of OG dye constant at 20 mg/L while varying the concentration
524 of coexisting ions (PO_4^{2-}, SO_4^{2-}, CO_3^{2-} and NO_3^-) from 20 to 60 mg/L. The operating

conditions were pH=6.0, adsorbent dose=0.5 g/L, contact time= 3 h and T = 25 °C. **Fig. 6(a)** shows the effect of coexisting ions on the performance of OG dye removal by PANI@Fe-ZSM-5 composite (Laabd et al., 2021). The presence of SO_4^{2-}, CO_3^{2-} and NO_3^- ions did not influence the OG removal and the adsorption capacity remained at 37.15 mg/g. In contrast, the presence of PO_4^{3-} ions had a considerable effect on the performance of OG adsorption. The increase of concentration of PO_4^{2-} resulted in a decrease of the amount of OG adsorbed until 17.03 mg/g. This adsorption behavior could be ascribed to the affinity of PANI@Fe-ZSM-5 surface for PO_4^{3-} ions, and subsequently the competition between OG dye and PO_4^{2-} anions significantly inhibited the OG adsorption (Banerjee et al., 2019).

For regeneration and reuse of PANI@Fe-ZSM-5, NaOH (0.5 M) was used as a regenerating agent. Further, it was reported in the literature that NaOH is the best suitable agent for desorbing OG dye from the adsorbent surfaces (Brini et al., 2021a; Hsini et al., 2021c; Xu et al., 2020). In this study, the recyclability of PANI@Fe-ZSM-5 composite for OG dye removal efficiency was evaluated up to five adsorption-desorption cycles. **Fig. 6(b)** depicts that the adsorption efficiency of OG dye from aqueous solutions was still above 86–% in the first four desorption/adsorption cycles. However, in the fifth regeneration cycle, the OG dye removal performance (38%) decreases significantly owing to the possible accumulation of OG molecules on the PANI@Fe-ZSM-5 surface. Overall, the experimental results revealed that the PANI@Fe-ZSM-5 composite owns excellent reusability and could be reused as an efficient and inexpensive adsorbent to eliminate of OG dye from aqueous solutions.

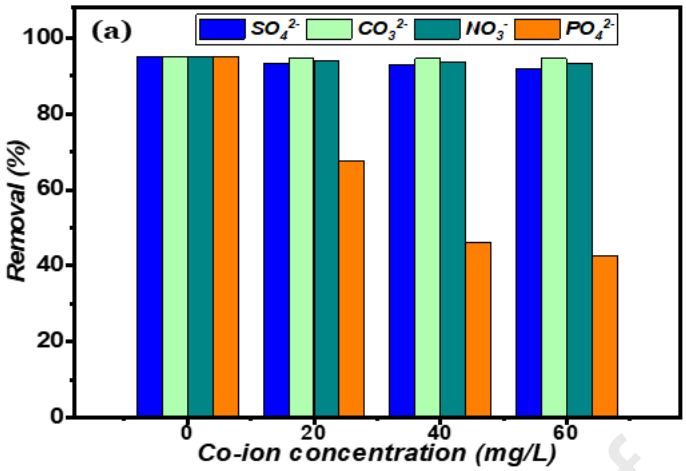
(a)
SO_4^{2-}
CO_3^{2-}
NO_3^-
PO_4^{2-}
Removal (%)
Co-ion concentration (mg/L)

547

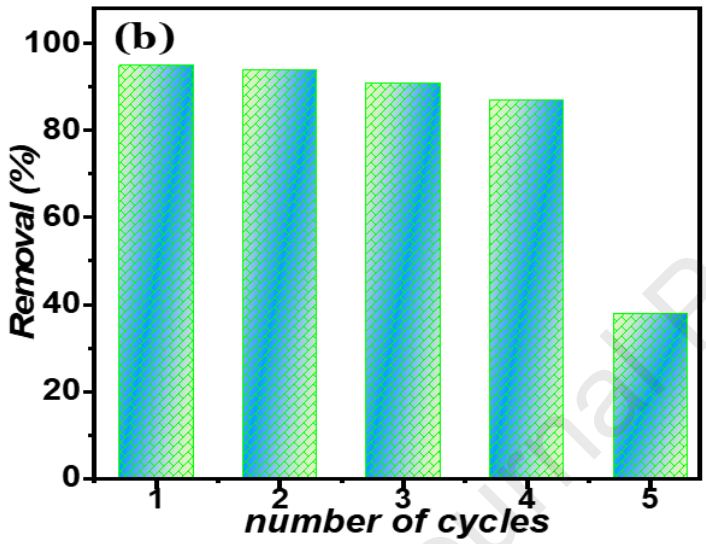
(b)
Removal (%)
number of cycles

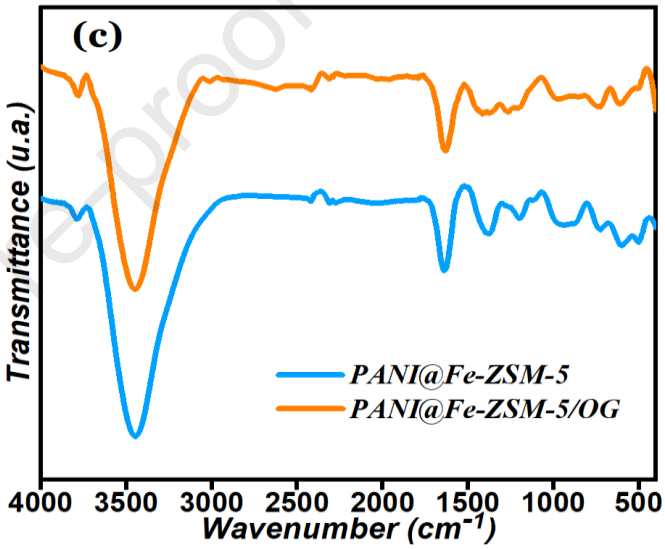
(c)
Transmittance (u.a.)
PANI@Fe-ZSM-5
PANI@Fe-ZSM-5/OG
Wavenumber (cm^{-1})

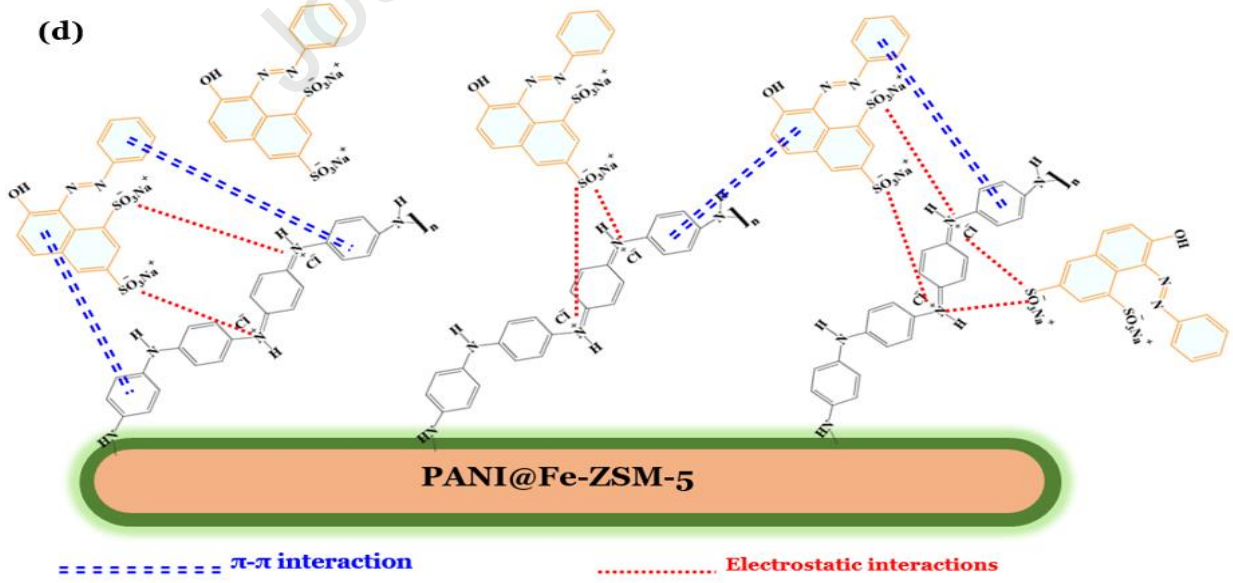
(d)
PANI@Fe-ZSM-5
π-π interaction
Electrostatic interactions

548

549 **Fig. 6. (a)** Effect of coexisting ions on the removal of OG dye by PANI@Fe-ZSM-5:
550 adsorbent dose = 0.5 g/L; pH= 6.0; 20 mg/L OG dye concentration; T=25°C**; (b)**
551 Adsorption efficiency of OG dye by PANI@Fe-ZSM-5 composite for 5 regeneration
552 cycles; **(c)** FT-IR spectral data of PANI@Fe-ZSM-5 before and after adsorption of OG
553 dye, and **(d)** Schematic ~~presentation~~ of the proposed adsorption mechanism.

554 ### 3.7. Comparison with other adsorbents

555 To evaluate the adsorption performance of PANI@Fe-ZSM-5, it is important to figure out
556 its position compared with other adsorbents. From a literature survey, many studies
557 reported the OG dye adsorption from water using different adsorbent materials. As shown
558 in **Table 1**, it is evident that the PANI@Fe-ZSM-5 composite demonstrated an excellent
559 maximum uptake capacity (217 mg/g) for OG dye removal compared with reported
560 adsorbents. Thus, we conclude that the as-synthesized adsorbent may be a useful material
561 for efficient OG dye removal. Finally, the as-developed PANI@Fe-ZSM-5 hybrid material
562 can be recommended as a potential and inexpensive adsorbent to clean up OG dye from
563 wastewaters.

564 **Table 1.** Comparison of the maximum uptake capacities of PANI@Fe-ZSM-5 for OG
565 removal and other adsorbents addressed in the previously published studies.

566

567

568

Adsorbent	Q_{max} (mg g^{-1})	Operating conditions			Reference
		Equilibrium time (min)	Dose (g L^{-1})	pH	
FSMD MNPs	109.1	60	1	3	(Zheng et al., 2019)
Alumina nanoparticles	93.3	45	1	2.5	(Banerjee et al., 2019)
Cts(x)-g-PNVP	63.7	175	10	3	(Sutirman et al., 2019)
Monoamine-modified silica	36.3	300	1	3	(Donia et al., 2009)
Prussian-Blue nanoparticles supported over alumina	44.4	100	6.5	3	(Doumic et al., 2015)
AC from coffee grounds	100	180	1	3	(Laksaci et al., 2019)
Modified montmorillonite nanoclay	39.4	60	2.5	8	(Salam et al., 2017)
PANI@Walnut shells	17.24	90	1	6	(Imgharn et al., 2021)
Bagasse fly ash	18.79	200	2	4	(Mall et al., 2006)
Kapok fiber oriented polyaniline	192.3	240	1	6	(Zheng et al., 2012)
H-MIL -53(Fe)	163.9	300	--	4	(Feng et al., 2020)

PANI@AS biocomposite	190.98	100	0.5	5	(Hsini et al., 2020)
Cucumber peels	37.8	60	0.5	6	(Stavrinou et al., 2018)
PANI@Fe-ZSM-5 composite	**217**	120	0.5	5	**Current study**

Conclusion

In this contribution, PANI@Fe-ZSM-5 composite was synthesized, characterized and used for OG dye removal from water. The adsorption study established that the PANI@Fe-ZSM-5 composite as an effective adsorbent for the removal of OG dye from aqueous solutions. Based on the results obtained for pH influence on the adsorption process and PZC of PANI@Fe-ZSM-5 composite, electrostatic interactions were likely the main forces governing the OG dye adsorption mechanism. The kinetic data for OG dye removal by the PANI@Fe-ZSM-5 composite was well-fitted by the pseudo-second-order model. The mass transfer process of OG dye from the solution to the PANI@Fe-ZSM-5 surface occurred via three consecutive stages: (i) external diffusion, (ii) intraparticle diffusion and (iii) final adsorption equilibrium. The OG dye binding mechanism and associated thermodynamic behavior were evaluated on the basis of advanced statistical physics theory. Among the fitted statistical physics models to the experimental findings, the **M3** model (monolayer layer model with the different energy sites) is the best one to describe the OG dye adsorption process. Based on this model, the macroscopic and microscopic aspects related to the adsorption system were assessed. The OG dye molecules were adsorbed in the perpendicular (multi-docking) and parallel (multimolecular) modes on the first ($n_1 < 1$)

and second ($n_2 > 1$) types of active sites in the PANI@Fe-ZSM-5 surface. The thermodynamic functions confirmed the feasibility of OG adsorption onto PANI@Fe-ZSM-5 composite through physical interactions. The theoretical data are in satisfactory concordance with experimental results. Finally, we can conclude that the as-developed PANI@Fe-ZSM-5 material can be applied as an efficient and regenerable adsorbent for treating the textile effluents.

References

Abbasi, M., 2017. Synthesis and characterization of magnetic nanocomposite of chitosan/SiO_2/carbon nanotubes and its application for dyes removal. J. Clean. Prod. 145, 105–113. https://doi.org/10.1016/j.jclepro.2017.01.046

Abdel Hamid, Z., Hasan Gomaa, M., S. Abdel Rehim, S., Abdel Hamid, M., Ibrahim, A., 2019. Synthesis and Characterization of Nanostructured Polyaniline Thin Films with Superhydrophobic Properties. Coatings 9, 748. https://doi.org/10.3390/coatings9110748

Abdellaoui, Y., Gamero-Melo, P., Díaz-Jiménez, L., Ponce-Caballero, C., Giácoman-Vallejos, G., 2020. Synthesis and Surface Modification of Small Pore Size Zeolite W for Improving Removal Efficiency of Anionic Contaminants from Water. Bull. Environ. Contam. Toxicol. 105, 934–940. https://doi.org/10.1007/s00128-020-03036-z

Ait Haki, M., Imgharn, A., Aarab, N., Hsini, A., Essekri, A., Laabd, M., El Jazouli, H., Elamine, M., Lakhmiri, R., Albourine, A., 2021. Efficient removal of crystal violet dye from aqueous solutions using sodium hydroxide modified avocado shells: kinetics and isotherms modeling. Water Sci. Technol. wst2021451. https://doi.org/10.2166/wst.2021.451

Akhsassi, B., Bouddouch, A., Naciri, Y., Bakiz, B., Taoufyq, A., Favotto, C., Villain, S., Guinneton, F., Benlhachemi, A., 2021. Enhanced photocatalytic activity of $Zn_3(PO_4)_2$/ZnO composite semiconductor prepared by different methods. Chem. Phys. Lett. 783, 139046. https://doi.org/10.1016/j.cplett.2021.139046

Amjlef, A., Khrach, S., Ait El Fakir, A., Farsad, S., Et-Taleb, S., El Alem, N., 2021. Adsorptive properties investigation of natural sand as adsorbent for methylene blue removal from contaminated water. Nanotechnol. Environ. Eng. 6, 26. https://doi.org/10.1007/s41204-021-00119-y

Ansari, M.O., Kumar, R., Ansari, S.A., Ansari, S.P., Barakat, M.A., Alshahrie, A., Cho, M.H., 2017. Anion selective pTSA doped polyaniline@graphene oxide-multiwalled carbon nanotube composite for Cr(VI) and Congo red adsorption. J. Colloid Interface Sci. 496, 407–415. https://doi.org/10.1016/j.jcis.2017.02.034

Ayachi, F., Z. Kyzas, G., Aatrous, M., Sakly, A., Ben Lamine, A., 2019. Evaluating the adsorption of Ni(II) and Cu(II) on spirulina biomass by statistical physics

formalism. J. Ind. Eng. Chem. 80, 461–470. https://doi.org/10.1016/j.jiec.2019.05.044

Ba Mohammed, B., Hsini, A., Abdellaoui, Y., Abou Oualid, H., Laabd, M., El Ouardi, M., Ait Addi, A., Yamni, K., Tijani, N., 2020. Fe-ZSM-5 zeolite for efficient removal of basic Fuchsin dye from aqueous solutions: Synthesis, characterization and adsorption process optimization using BBD-RSM modeling. J. Environ. Chem. Eng. 8, 104419. https://doi.org/10.1016/j.jece.2020.104419

Banerjee, S., Dubey, S., Gautam, R.K., Chattopadhyaya, M.C., Sharma, Y.C., 2019. Adsorption characteristics of alumina nanoparticles for the removal of hazardous dye, Orange G from aqueous solutions. Arab. J. Chem. 12, 5339–5354. https://doi.org/10.1016/j.arabjc.2016.12.016

Belbachir, I., Makhoukhi, B., 2017. Adsorption of Bezathren dyes onto sodic bentonite from aqueous solutions. J. Taiwan Inst. Chem. Eng. 75, 105–111. https://doi.org/10.1016/j.jtice.2016.09.042

Benjelloun, M., Miyah, Y., Akdemir Evrendilek, G., Zerrouq, F., Lairini, S., 2021. Recent Advances in Adsorption Kinetic Models: Their Application to Dye Types. Arab. J. Chem. 14, 103031. https://doi.org/10.1016/j.arabjc.2021.103031

Bhaumik, M., Maity, A., Brink, H.G., 2021. Zero valent nickel nanoparticles decorated polyaniline nanotubes for the efficient removal of Pb(II) from aqueous solution: Synthesis, characterization and mechanism investigation. Chem. Eng. J. 417, 127910. https://doi.org/10.1016/j.cej.2020.127910

Brini, L., H'Maida, K., Imgharn, A., Hsini, A., Naciri, Y., Ajmal, Z., Bouziani, A., Boulahya, A., Arahou, M., Bakiz, B., Albourine, A., Fekhaoui, M., 2021a. Synthesis and characterisation of PANI- coated Heliotrope Leaves (PANI@HL) with high clean-up capacity for Orange G dye from aqueous media. Int. J. Environ. Anal. Chem. 1–17. https://doi.org/10.1080/03067319.2021.1994557

Brini, L., Hsini, A., Naciri, Y., Bouziani, A., Ajmal, Z., H'Maida, K., Boulahya, A., Arahou, M., Bakiz, B., Albourine, A., Fekhaoui, M., 2021b. Synthesis and characterization of arginine-doped heliotrope leaves with high clean-up capacity for crystal violet dye from aqueous media. Water Sci. Technol. 84, 2265–2277. https://doi.org/10.2166/wst.2021.446

Chan, H.S.O., Ng, S.C., Sim, W.S., Tan, K.L., Tan, B.T.G., 1992. Preparation and characterization of electrically conducting copolymers of aniline and anthranilic acid: evidence for self-doping by x-ray photoelectron spectroscopy. Macromolecules 25, 6029–6034. https://doi.org/10.1021/ma00048a026

Donia, A.M., Atia, A.A., Al-amrani, W.A., El-Nahas, A.M., 2009. Effect of structural properties of acid dyes on their adsorption behaviour from aqueous solutions by amine modified silica. J. Hazard. Mater. 161, 1544–1550. https://doi.org/10.1016/j.jhazmat.2008.05.042

Doula, M.K., 2007. Synthesis of a clinoptilolite–Fe system with high Cu sorption capacity. Chemosphere 67, 731–740. https://doi.org/10.1016/j.chemosphere.2006.10.072

Doumic, L., Salierno, G., Cassanello, M., Haure, P., Ayude, M., 2015. Efficient removal of Orange G using Prussian Blue nanoparticles supported over alumina. Catal. Today 240, 67–72. https://doi.org/10.1016/j.cattod.2014.03.064

Fahoul, Y., Tanji, K., Zouheir, M., Mrabet, I.E., Naciri, Y., Hsini, A., Nahali, L., Kherbeche, A., 2022. Novel River Sediment@ZnO Co nanocomposite for

photocatalytic degradation and COD reduction of crystal violet under visible light. J. Mol. Struct. 1253, 132298. https://doi.org/10.1016/j.molstruc.2021.132298

Feng, T., Bavumiragira, J.P., Wambui, M.A., Kabtamu, D.M., László, K., Wang, Y., Li, F., 2020. Hierarchical porous induced competent removal of low concentration azo dye molecules by generating a leachy crystalline structure H-MIL-53(Fe). Chin. Chem. Lett. 31, 2717–2720. https://doi.org/10.1016/j.cclet.2020.04.044

Fiol, N., Villaescusa, I., 2009. Determination of sorbent point zero charge: usefulness in sorption studies. Environ. Chem. Lett. 7, 79–84. https://doi.org/10.1007/s10311-008-0139-0

Gottlieb, A., Shaw, C., Smith, A., Wheatley, A., Forsythe, S., 2003. The toxicity of textile reactive azo dyes after hydrolysis and decolourisation. J. Biotechnol. 101, 49–56. https://doi.org/10.1016/S0168-1656(02)00302-4

Hassan, M.M., Carr, C.M., 2018. A critical review on recent advancements of the removal of reactive dyes from dyehouse effluent by ion-exchange adsorbents. Chemosphere 209, 201–219. https://doi.org/10.1016/j.chemosphere.2018.06.043

Hsini, A., Benafqir, M., Naciri, Y., Laabd, M., Bouziani, A., Ez-zahery, M., Lakhmiri, R., Alem, N.E., Albourine, A., 2021a. Synthesis of an arginine-functionalized polyaniline@FeOOH composite with high removal performance of hexavalent chromium ions from water: Adsorption behavior, regeneration and process capability studies. Colloids Surf. Physicochem. Eng. Asp. 617, 126274. https://doi.org/10.1016/j.colsurfa.2021.126274

Hsini, A., Essekri, A., Aarab, N., Laabd, M., Ait Addi, A., Lakhmiri, R., Albourine, A., 2020. Elaboration of novel polyaniline@Almond shell biocomposite for effective removal of hexavalent chromium ions and Orange G dye from aqueous solutions. Environ. Sci. Pollut. Res. 27, 15245–15258. https://doi.org/10.1007/s11356-020-08039-1

Hsini, A., Naciri, Y., Benafqir, M., Ajmal, Z., Aarab, N., Laabd, M., Navío, J.A., Puga, F., Boukherroub, R., Bakiz, B., Albourine, A., 2021b. Facile synthesis and characterization of a novel 1,2,4,5-benzene tetracarboxylic acid doped polyaniline@zinc phosphate nanocomposite for highly efficient removal of hazardous hexavalent chromium ions from water. J. Colloid Interface Sci. 585, 560–573. https://doi.org/10.1016/j.jcis.2020.10.036

Hsini, A., Naciri, Y., Bouziani, A., Aarab, N., Essekri, A., Imgharn, A., Laabd, M., Navío, J.A., Puga, F., Lakhmiri, R., Albourine, A., 2021c. Polyaniline coated tungsten trioxide as an effective adsorbent for the removal of orange G dye from aqueous media. RSC Adv. 11, 31272–31283. https://doi.org/10.1039/D1RA04135E

Hsini, A., Naciri, Y., Laabd, M., Bouziani, A., Navío, J.A., Puga, F., Boukherroub, R., Lakhmiri, R., Albourine, A., 2021d. Development of a novel PANI@WO_3 hybrid composite and its application as a promising adsorbent for Cr(VI) ions removal. J. Environ. Chem. Eng. 9, 105885. https://doi.org/10.1016/j.jece.2021.105885

Imgharn, A., ighnih, H., Hsini, A., Naciri, Y., Laabd, M., Kabli, H., Elamine, M., Lakhmiri, R., Souhail, B., Albourine, A., 2021. Synthesis and characterization of polyaniline-based biocomposites and their application for effective removal of Orange G dye using Adsorption in dynamic regime. Chem. Phys. Lett. 138811. https://doi.org/10.1016/j.cplett.2021.138811

Kachangoon, R., Vichapong, J., Santaladchaiyakit, Y., Burakham, R., Srijaranai, S., 2020. An Eco-Friendly Hydrophobic Deep Eutectic Solvent-Based Dispersive Liquid–Liquid Microextraction for the Determination of Neonicotinoid Insecticide Residues in Water, Soil and Egg Yolk Samples. Molecules 25, 2785. https://doi.org/10.3390/molecules25122785

Khalfaoui, M., Ghali, A.E., Aguir, C., Mohamed, Z., Baouab, M.H.V., Lamine, A.B., 2015. Study on adsorption of herbicide onto functionalized cellulose extracted from Juncus acutus L. plant: Experimental results and theoretical modeling. Ind. Crops Prod. 67, 169–178. https://doi.org/10.1016/j.indcrop.2015.01.032

Kumar, P.A., Chakraborty, S., Ray, M., 2008. Removal and recovery of chromium from wastewater using short chain polyaniline synthesized on jute fiber. Chem. Eng. J. 141, 130–140. https://doi.org/10.1016/j.cej.2007.11.004

Laabd, M., Brahmi, Y., El Ibrahimi, B., Hsini, A., Toufik, E., Abdellaoui, Y., Abou Oualid, H., El Ouardi, M., Albourine, A., 2021. A novel mesoporous Hydroxyapatite@Montmorillonite hybrid composite for high-performance removal of emerging Ciprofloxacin antibiotic from water: Integrated experimental and Monte Carlo computational assessment. J. Mol. Liq. 338, 116705. https://doi.org/10.1016/j.molliq.2021.116705

Laabd, M., Chafai, H., Essekri, A., Elamine, M., Al-Muhtaseb, S.A., Lakhmiri, R., Albourine, A., 2017. Single and multi-component adsorption of aromatic acids using an eco-friendly polyaniline-based biocomposite. Sustain. Mater. Technol. 12, 35–43. https://doi.org/10.1016/j.susmat.2017.04.004

Laabd, M., Imgharn, A., Hsini, A., Naciri, Y., Mobarak, M., Szunerits, S., Boukherroub, R., Albourine, A., 2022. Efficient detoxification of Cr(VI)-containing effluents by sequential adsorption and reduction using a novel cysteine-doped PANi@faujasite composite: Experimental study supported by advanced statistical physics prediction. J. Hazard. Mater. 422, 126857. https://doi.org/10.1016/j.jhazmat.2021.126857

Laksaci, H., Khelifi, A., Belhamdi, B., Trari, M., 2019. The use of prepared activated carbon as adsorbent for the removal of orange G from aqueous solution. Microchem. J. 145, 908–913. https://doi.org/10.1016/j.microc.2018.12.001

Li, Z., Sellaoui, L., Dotto, G.L., Lamine, A.B., Bonilla-Petriciolet, A., Hanafy, H., Belmabrouk, H., Netto, M.S., Erto, A., 2019. Interpretation of the adsorption mechanism of Reactive Black 5 and Ponceau 4R dyes on chitosan/polyamide nanofibers via advanced statistical physics model. J. Mol. Liq. 285, 165–170. https://doi.org/10.1016/j.molliq.2019.04.091

Liao, G., Li, Q., Xu, Z., 2019. The chemical modification of polyaniline with enhanced properties: A review. Prog. Org. Coat. 126, 35–43. https://doi.org/10.1016/j.porgcoat.2018.10.018

Liu, G., Xiangli, F., Wei, W., Liu, S., Jin, W., 2011. Improved performance of PDMS/ceramic composite pervaporation membranes by ZSM-5 homogeneously dispersed in PDMS via a surface graft/coating approach. Chem. Eng. J. 174, 495–503. https://doi.org/10.1016/j.cej.2011.06.004

Mall, I.D., Srivastava, V.C., Agarwal, N.K., 2006. Removal of Orange-G and Methyl Violet dyes by adsorption onto bagasse fly ash—kinetic study and equilibrium isotherm analyses. Dyes Pigments 69, 210–223. https://doi.org/10.1016/j.dyepig.2005.03.013

765 Mimouni, I., Bouziani, A., Naciri, Y., Boujnah, M., El Belghiti, M.A., El Azzouzi, M.,
766 2021. Effect of heat treatment on the photocatalytic activity of α-Fe_2O_3
767 nanoparticles: towards diclofenac elimination. Environ. Sci. Pollut. Res.
768 https://doi.org/10.1007/s11356-021-16146-w
769 Mobarak, M., Mohamed, E.A., Selim, A.Q., Eissa, M.F., Seliem, M.K., 2019a.
770 Experimental results and theoretical statistical modeling of malachite green
771 adsorption onto MCM–41 silica/rice husk composite modified by beta radiation.
772 J. Mol. Liq. 273, 68–82. https://doi.org/10.1016/j.molliq.2018.09.132
773 Mobarak, M., Mohamed, E.A., Selim, A.Q., Mohamed, F.M., Sellaoui, L., Bonilla-
774 Petriciolet, A., Seliem, M.K., 2019b. Statistical physics modeling and
775 interpretation of methyl orange adsorption on high–order mesoporous composite
776 of MCM–48 silica with treated rice husk. J. Mol. Liq. 285, 678–687.
777 https://doi.org/10.1016/j.molliq.2019.04.116
778 Mohamed, E.A., Mobarak, M., Kumar, R., Barakat, M.A., Bonilla-Petriciolet, A., Seliem,
779 M.K., Selim, A.Q., 2020. Novel hybrid multifunctional composite of chitosan and
780 altered basalt for barium adsorption: Experimental and theoretical studies.
781 Colloids Surf. Physicochem. Eng. Asp. 593, 124613.
782 https://doi.org/10.1016/j.colsurfa.2020.124613
783 Naciri, Y., Hsini, A., Bouziani, A., Djellabi, R., Ajmal, Z., Laabd, M., Navío, J.A., Mills, A.,
784 Bianchi, C.L., Li, H., Bakiz, B., Albourine, A., 2021. Photocatalytic oxidation of
785 pollutants in gas-phase via Ag_3PO_4 -based semiconductor photocatalysts: Recent
786 progress, new trends, and future perspectives. Crit. Rev. Environ. Sci. Technol. 1–
787 44. https://doi.org/10.1080/10643389.2021.1877977
788 Naciri, Y., Hsini, A., Bouziani, A., Tanji, K., El Ibrahimi, B., Ghazzal, M.N., Bakiz, B.,
789 Albourine, A., Benlhachemi, A., Navío, J.A., Li, H., 2022. Z-scheme WO_3/PANI
790 heterojunctions with enhanced photocatalytic activity under visible light: A depth
791 experimental and DFT studies. Chemosphere 292, 133468.
792 https://doi.org/10.1016/j.chemosphere.2021.133468
793 Narayanan, S., Vijaya, J.J., Sivasanker, S., Kennedy, L.J., Jesudoss, S.K., 2015.
794 Structural, morphological and catalytic investigations on hierarchical ZSM-5
795 zeolite hexagonal cubes by surfactant assisted hydrothermal method. Powder
796 Technol. 274, 338–348. https://doi.org/10.1016/j.powtec.2015.01.054
797 Nasar, A., Mashkoor, F., 2019. Application of polyaniline-based adsorbents for dye
798 removal from water and wastewater—a review. Environ. Sci. Pollut. Res. 26,
799 5333–5356. https://doi.org/10.1007/s11356-018-3990-y
800 Niu, X.R., Li, J., Zhang, L., Lei, Z.T., Zhao, X.L., Yang, C.H., 2017. ZSM-5 functionalized
801 in situ with manganese ions for the catalytic oxidation of cyclohexane. RSC Adv 7,
802 50619–50625. https://doi.org/10.1039/C7RA10771D
803 Njoya, O., Zhao, S., Qu, Y., Shen, J., Wang, B., Shi, H., Chen, Z., 2020. Performance and
804 potential mechanism of Cr(VI) reduction and subsequent Cr(III) precipitation
805 using sodium borohydride driven by oxalate. J. Environ. Manage. 275, 111165.
806 https://doi.org/10.1016/j.jenvman.2020.111165
807 Ravelo-Acuña, D., Fuentes-García, J.A., Yee-Madeira, H.T., Diaz-Cano, A.I., Goya, G.F.,
808 Santoyo-Salazar, J., 2019. Sonochemical magnetite encapsulation in silica at low
809 irradiation power. Mater. Lett. 250, 103–107.
810 https://doi.org/10.1016/j.matlet.2019.04.073

Renault, F., Sancey, B., Badot, P.-M., Crini, G., 2009. Chitosan for coagulation/flocculation processes – An eco-friendly approach. Eur. Polym. J. 45, 1337–1348. https://doi.org/10.1016/j.eurpolymj.2008.12.027

Sahu, S., Sahu, U.K., Patel, R.K., 2019. Modified Thorium Oxide Polyaniline Core–Shell Nanocomposite and Its Application for the Efficient Removal of Cr(VI). J. Chem. Eng. Data 64, 1294–1304. https://doi.org/10.1021/acs.jced.8b01225

Saifuddin, M., Bae, J., Kim, K.S., 2019. Role of Fe, Na and Al in Fe-Zeolite-A for adsorption and desorption of phosphate from aqueous solution. Water Res. 158, 246–256. https://doi.org/10.1016/j.watres.2019.03.045

Salam, M.A., Kosa, S.A., Al-Beladi, A.A., 2017. Application of nanoclay for the adsorptive removal of Orange G dye from aqueous solution. J. Mol. Liq. 241, 469–477. https://doi.org/10.1016/j.molliq.2017.06.055

Seliem, M.K., Mobarak, M., 2019. Cr(VI) uptake by a new adsorbent of CTAB–modified carbonized coal: Experimental and advanced statistical physics studies. J. Mol. Liq. 294, 111676. https://doi.org/10.1016/j.molliq.2019.111676

Sellaoui, L., Depci, T., Kul, A.R., Knani, S., Ben Lamine, A., 2016. A new statistical physics model to interpret the binary adsorption isotherms of lead and zinc on activated carbon. J. Mol. Liq. 214, 220–230. https://doi.org/10.1016/j.molliq.2015.12.080

Sellaoui, L., Dotto, G.L., Wjihi, S., Gonçalves, J.O., Pinto, L.A.A., Lamine, A.B., Erto, A., 2017a. Thermodynamic analysis of single and binary adsorption of Food Yellow 4 and Food Blue 2 on CC-chitosan: Application of statistical physics and IAST models. J. Mol. Liq. 232, 499–505. https://doi.org/10.1016/j.molliq.2017.02.103

Sellaoui, L., Guedidi, H., Knani, S., Reinert, L., Duclaux, L., Ben Lamine, A., 2015. Application of statistical physics formalism to the modeling of adsorption isotherms of ibuprofen on activated carbon. Fluid Phase Equilibria 387, 103–110. https://doi.org/10.1016/j.fluid.2014.12.018

Sellaoui, L., Mechi, N., Lima, É.C., Dotto, G.L., Ben Lamine, A., 2017b. Adsorption of diclofenac and nimesulide on activated carbon: Statistical physics modeling and effect of adsorbate size. J. Phys. Chem. Solids 109, 117–123. https://doi.org/10.1016/j.jpcs.2017.05.019

Shyaa, A.A., Hasan, O.A., Abbas, A.M., 2015. Synthesis and characterization of polyaniline/zeolite nanocomposite for the removal of chromium(VI) from aqueous solution. J. Saudi Chem. Soc. 19, 101–107. https://doi.org/10.1016/j.jscs.2012.01.001

Stavrinou, A., Aggelopoulos, C.A., Tsakiroglou, C.D., 2018. Exploring the adsorption mechanisms of cationic and anionic dyes onto agricultural waste peels of banana, cucumber and potato: Adsorption kinetics and equilibrium isotherms as a tool. J. Environ. Chem. Eng. 6, 6958–6970. https://doi.org/10.1016/j.jece.2018.10.063

Suresh, R., Giribabu, K., Manigandan, R., Stephen, A., Narayanan, V., 2014. Fabrication of Ni–Fe2O3 magnetic nanorods and application to the detection of uric acid. RSC Adv. 4, 17146. https://doi.org/10.1039/c4ra00725e

Sutirman, Z.A., Sanagi, M.M., Abd Karim, K.J., Abu Naim, A., Wan Ibrahim, W.A., 2019. Enhanced removal of Orange G from aqueous solutions by modified chitosan beads: Performance and mechanism. Int. J. Biol. Macromol. 133, 1260–1267. https://doi.org/10.1016/j.ijbiomac.2019.04.188

857 Tang, D., Zhang, G., 2016. Efficient removal of fluoride by hierarchical Ce–Fe bimetal
858 oxides adsorbent: Thermodynamics, kinetics and mechanism. Chem. Eng. J. 283,
859 721–729. https://doi.org/10.1016/j.cej.2015.08.019
860 Tu, B., Wen, R., Wang, K., Cheng, Y., Deng, Y., Cao, W., Zhang, K., Tao, H., 2020.
861 Efficient removal of aqueous hexavalent chromium by activated carbon derived
862 from Bermuda grass. J. Colloid Interface Sci. 560, 649–658.
863 https://doi.org/10.1016/j.jcis.2019.10.103
864 Wang, Q., Qiu, S., Wang, S., Shang, J., Zhao, R., Wu, X., Chen, W., Zhou, H., Wang, X.,
865 2015. Graphene oxide/polyaniline nanotube composites synthesized in alkaline
866 aqueous solution. Synth. Met. 210, 314–322.
867 https://doi.org/10.1016/j.synthmet.2015.10.017
868 Wang, X., Liu, N., Yan, X., Zhang, W., Wei, Y., 2005. Alkali-guided Synthesis of
869 Polyaniline Hollow Microspheres. Chem. Lett. 34, 42–43.
870 https://doi.org/10.1246/cl.2005.42
871 Wjihi, S., Aouaini, F., Almuqrin, A.H., Lamine, A.B., 2020. Physicochemical assessment
872 of prednisone adsorption on two molecular composites using statistical physics
873 formalism in cosmetics. Arab. J. Chem. 13, 6876–6886.
874 https://doi.org/10.1016/j.arabjc.2020.06.040
875 Wjihi, S., Sellaoui, L., Bouzid, M., Dhaou, H., Knani, S., Jemni, A., Ben Lamine, A., 2017.
876 Theoretical study of hydrogen sorption on $LaNi_5$ using statistical physics
877 treatment: microscopic and macroscopic investigation. Int. J. Hydrog. Energy 42,
878 2699–2712. https://doi.org/10.1016/j.ijhydene.2016.10.102
879 Xu, H., Zhang, J., Chen, Y., Lu, H., Zhuang, J., Li, J., 2014. Synthesis of polyaniline-
880 modified MnO_2 composite nanorods and their photocatalytic application. Mater.
881 Lett. 117, 21–23. https://doi.org/10.1016/j.matlet.2013.11.089
882 Xu, M.-Y., Jiang, H.-L., Xie, Z.-W., Li, Z.-T., Xu, D., He, F.-A., 2020. Highly efficient
883 selective adsorption of anionic dyes by modified β-cyclodextrin polymers. J.
884 Taiwan Inst. Chem. Eng. 108, 114–128.
885 https://doi.org/10.1016/j.jtice.2020.01.005
886 Yeamin, Md.B., Islam, Md.M., Chowdhury, A.-N., Awual, Md.R., 2021. Efficient
887 encapsulation of toxic dyes from wastewater using several biodegradable natural
888 polymers and their composites. J. Clean. Prod. 291, 125920.
889 https://doi.org/10.1016/j.jclepro.2021.125920
890 Zhang, J., Gao, J., Song, Q., Guo, Z., Chen, A., Chen, G., Zhou, S., 2016. N-substituted
891 Carboxyl Polyaniline Covalent Grafting Reduced Graphene Oxide
892 Nanocomposites and Its Application in Supercapacitor. Electrochimica Acta 199,
893 70–79. https://doi.org/10.1016/j.electacta.2016.03.003
894 Zheng, X., Zheng, H., Zhou, Y., Sun, Y., Zhao, R., Liu, Y., Zhang, S., 2019. Enhanced
895 adsorption of Orange G from aqueous solutions by quaternary ammonium group-
896 rich magnetic nanoparticles. Colloids Surf. Physicochem. Eng. Asp. 580, 123746.
897 https://doi.org/10.1016/j.colsurfa.2019.123746
898 Zheng, Y., Liu, Y., Wang, A., 2012. Kapok Fiber Oriented Polyaniline for Removal of
899 Sulfonated Dyes. Ind. Eng. Chem. Res. 51, 10079–10087.
900 https://doi.org/10.1021/ie300246m
901 Zhou, T., Li, C., Jin, H., Lian, Y., Han, W., 2017. Effective Adsorption/Reduction of
902 Cr(VI) Oxyanion by Halloysite@Polyaniline Hybrid Nanotubes. ACS Appl. Mater.
903 Interfaces 9, 6030–6043. https://doi.org/10.1021/acsami.6b14079

904

Highlights

- ✓ A novel PANI@Fe-ZSM-5 hybrid composite was easily elaborated and fully characterized.
- ✓ The adsorption performance of PANI@Fe-ZSM-5 towards OG dye was investigated.
- ✓ The OG dye binding mechanism was assessed by advanced statistical physics modeling.
- ✓ Statistical physics parameters and thermodynamic functions of the adsorption system were studied.
- ✓ PANI@Fe-ZSM-5 composite has excellent adsorption ability and satisfactory reusability.

Declaration of Interest Statement

- The authors declare that they have no known competing financial interests or personal relationships that could have appeared to influence the work reported in this paper.